
























































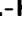


































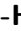
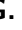














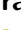






























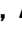




































































































PREPARED FOR SUBMISSION TO JHEP

Determination of the CKM angle ϕ_3 from a combination of Belle and Belle II results

The Belle and Belle II Collaborations

I. Adachi , L. Aggarwal , H. Aihara , N. Akopov , A. Aloisio , S. Al Said ,
N. Anh Ky , D. M. Asner , H. Atmacan , V. Aushev , M. Aversano , R. Ayad ,
V. Babu , H. Bae , S. Bahinipati , P. Bambade , Sw. Banerjee , S. Bansal ,
M. Barrett , J. Baudot , A. Baur , A. Beaubien , F. Becherer , J. Becker ,
K. Belous , J. V. Bennett , F. U. Bernlochner , V. Bertacchi , M. Bertemes ,
E. Bertholet , M. Bessner , S. Bettarini , B. Bhuyan , F. Bianchi ,
L. Bierwirth , T. Bilka , S. Bilokin , D. Biswas , A. Bobrov , D. Bodrov ,
A. Bolz , A. Bondar , A. Bozek , M. Bračko , P. Branchini , R. A. Briere ,
T. E. Browder , A. Budano , S. Bussino , M. Campajola , L. Cao ,
G. Casarosa , C. Cecchi , J. Cerasoli , M.-C. Chang , P. Chang , R. Cheaib ,
P. Cheema , B. G. Cheon , K. Chilikin , K. Chirapatpimol , H.-E. Cho ,
K. Cho , S.-K. Choi , Y. Choi , S. Choudhury , L. Corona , S. Das ,
F. Dattola , E. De La Cruz-Burelo , S. A. De La Motte , G. de Marino ,
G. De Nardo , M. De Nuccio , G. De Pietro , R. de Sangro , M. Destefanis ,
R. Dhamija , A. Di Canto , F. Di Capua , J. Dingfelder , Z. Doležal ,
T. V. Dong , M. Dorigo , K. Dort , D. Dossett , S. Dreyer , S. Dubey ,
G. Dujany , P. Ecker , M. Eliachevitch , D. Epifanov , P. Feichtinger ,
T. Ferber , D. Ferlewicz , T. Fillinger , G. Finocchiaro , A. Fodor , F. Forti ,
A. Frey , B. G. Fulsom , A. Gabrielli , E. Ganiev , M. Garcia-Hernandez ,
R. Garg , G. Gaudino , V. Gaur , A. Gaz , A. Gellrich , G. Ghevondyan ,
D. Ghosh , H. Ghumaryan , G. Giakoustidis , R. Giordano , A. Giri ,
B. Gobbo , R. Godang , O. Gogota , P. Goldenzweig , W. Gradl ,
T. Grammatico , S. Granderath , E. Graziani , D. Greenwald , Z. Gruberová ,
T. Gu , Y. Guan , K. Gudkova , S. Halder , Y. Han , T. Hara , H. Hayashii ,
S. Hazra , M. T. Hedges , A. Heidelberg , I. Heredia de la Cruz ,
M. Hernández Villanueva , T. Higuchi , M. Hoek , M. Hohmann , P. Horak ,
C.-L. Hsu , T. Humair , T. Iijima , K. Inami , N. Ipsita , A. Ishikawa ,
R. Itoh , M. Iwasaki , P. Jackson , W. W. Jacobs , E.-J. Jang , Q. P. Ji ,
S. Jia , Y. Jin , H. Junkerkalefeld , D. Kalita , A. B. Kaliyar , J. Kandra ,
T. Kawasaki , F. Keil , C. Kiesling , C.-H. Kim , D. Y. Kim , K.-H. Kim 

Y.-K. Kim , H. Kindo , K. Kinoshita , P. Kodyš , T. Koga , S. Kohani ,
 K. Kojima , A. Korobov , S. Korpar , E. Kovalenko , R. Kowalewski ,
 T. M. G. Kraetzschmar , P. Križan , P. Krovovny , T. Kuhr , J. Kumar ,
 M. Kumar , R. Kumar , K. Kumara , T. Kunigo , A. Kuzmin , Y.-J. Kwon ,
 S. Lacaprara , Y.-T. Lai , T. Lam , L. Lanceri , J. S. Lange , M. Laurenza ,
 M. J. Lee , D. Levit , P. M. Lewis , C. Li , L. K. Li , Y. Li , Y. B. Li ,
 J. Libby , M. H. Liu , Q. Y. Liu , Z. Q. Liu , D. Liventsev , S. Longo ,
 T. Lueck , C. Lyu , Y. Ma , M. Maggiora , S. P. Maharana , R. Maiti ,
 S. Maity , G. Mancinelli , R. Manfredi , E. Manoni , M. Mantovano ,
 D. Marcantonio , S. Marcello , C. Marinas , L. Martel , C. Martellini ,
 A. Martini , T. Martinov , L. Massaccesi , M. Masuda , D. Matvienko ,
 S. K. Maurya , J. A. McKenna , R. Mehta , F. Meier , M. Merola ,
 F. Metzner , C. Miller , M. Mirra , K. Miyabayashi , H. Miyake ,
 G. B. Mohanty , N. Molina-Gonzalez , S. Mondal , S. Moneta , H.-G. Moser ,
 M. Mrvar , R. Mussa , I. Nakamura , K. R. Nakamura , M. Nakao ,
 Y. Nakazawa , A. Narimani Charan , M. Naruki , D. Narwal , Z. Natkaniec ,
 A. Natochii , L. Nayak , M. Nayak , G. Nazaryan , M. Neu , C. Niebuhr ,
 S. Nishida , S. Ogawa , Y. Onishchuk , H. Ono , P. Oskin , F. Otani ,
 P. Pakhlov , G. Pakhlova , A. Panta , S. Pardi , K. Parham , H. Park ,
 S.-H. Park , A. Passeri , S. Patra , S. Paul , T. K. Pedlar , R. Peschke ,
 R. Pestotnik , M. Piccolo , L. E. Piilonen , G. Pinna Angioni ,
 P. L. M. Podesta-Lerma , T. Podobnik , S. Pokharel , C. Praz , S. Prell ,
 E. Prencipe , M. T. Prim , H. Purwar , P. Rados , G. Raeuber , S. Raiz ,
 N. Rauls , M. Reif , S. Reiter , M. Remnev , I. Ripp-Baudot , G. Rizzo ,
 S. H. Robertson , M. Roehrken , J. M. Roney , A. Rostomyan , N. Rout ,
 G. Russo , D. A. Sanders , S. Sandilya , L. Santelj , Y. Sato , V. Savinov ,
 B. Scavino , C. Schmitt , G. Schnell , C. Schwanda , M. Schwickardi ,
 Y. Seino , A. Selce , K. Senyo , J. Serrano , M. E. Sevier , C. Sfienti ,
 W. Shan , X. D. Shi , T. Shillington , T. Shimasaki , J.-G. Shiu , D. Shtol ,
 B. Shwartz , A. Sibidanov , F. Simon , J. B. Singh , J. Skorupa , R. J. Sobie ,
 M. Sobotzik , A. Soffer , A. Sokolov , E. Solovieva , S. Spataro , B. Spruck ,
 M. Starič , P. Stavroulakis , S. Stefkova , R. Stroili , M. Sumihama ,
 K. Sumisawa , W. Sutcliffe , N. Suwonjandee , M. Takizawa , U. Tamponi ,
 K. Tanida , F. Tenchini , O. Tittel , R. Tiwary , D. Tonelli , E. Torassa ,
 K. Trabelsi , I. Tsaklidis , M. Uchida , I. Ueda , Y. Uematsu , T. Uglov ,
 K. Unger , Y. Unno , K. Uno , S. Uno , P. Urquijo , Y. Ushiroda ,
 S. E. Vahsen , R. van Tonder , K. E. Varvell , M. Veronesi , A. Vinokurova ,
 V. S. Vismaya , L. Vitale , V. Vobbilisetti , R. Volpe , B. Wach , M. Wakai ,
 S. Wallner , E. Wang , M.-Z. Wang , X. L. Wang , Z. Wang , A. Warburton ,
 S. Watanuki , C. Wessel , E. Won , X. P. Xu , B. D. Yabsley , S. Yamada ,
 W. Yan , S. B. Yang , J. Yelton , J. H. Yin , K. Yoshihara , C. Z. Yuan ,
 B. Zhang , Y. Zhang , V. Zhilich , Q. D. Zhou , V. I. Zhukova ,

E-mail: coll-publications@belle2.org

ABSTRACT: We report a determination of the CKM angle ϕ_3 , also known as γ , from a combination of measurements using samples of up to 711 fb^{-1} from the Belle experiment and up to 362 fb^{-1} from the Belle II experiment. We combine results from analyses of $B^+ \rightarrow DK^+$, $B^+ \rightarrow D\pi^+$, and $B^+ \rightarrow D^*K^+$ decays, where D is an admixture of D^0 and \bar{D}^0 mesons, in a likelihood fit to obtain $\phi_3 = (75.2 \pm 7.6)^\circ$. We also briefly discuss the interpretation of this result.

ARXIV EPRINT: [2404.12817](https://arxiv.org/abs/2404.12817)

Contents

1	Introduction	1
2	Methods to obtain ϕ_3	2
3	Inputs from Belle and Belle II analyses	4
4	Auxiliary inputs	6
5	Statistical treatment	7
6	Results	8
6.1	Discussion	12
6.2	Coverage study	13
7	Summary	14

1 Introduction

The Cabibbo-Kobayashi-Maskawa (CKM) matrix [1, 2] describes weak interactions of quarks and accommodates the only source of charge-parity symmetry (CP) violation in the Standard Model (SM). The unitarity of the matrix can be represented as a triangle in the complex plane. One of its interior angles, ϕ_3 (also known as γ), is defined as $\phi_3 \equiv \arg(-V_{ud}V_{ub}^*/V_{cd}V_{cb}^*)$, where $V_{qq'}$ are CKM matrix elements. The angle ϕ_3 is of particular importance because it can be measured directly with negligible theoretical uncertainty by exploiting the interference between tree-level quark-transition amplitudes involving exchange of a single W -boson, $\bar{b} \rightarrow \bar{c}u\bar{s}$ and $\bar{b} \rightarrow \bar{u}c\bar{s}$ [3].¹ Hence, assuming only SM amplitudes in these processes, the measurement of ϕ_3 provides an accurate reference to be compared against indirect determinations from global unitarity fits. The latter resulting from combinations of measurements of the sides and the other two angles of the unitarity triangle can be modified by non-SM particles via transitions involving more than one vector boson [4]. The comparison between direct and indirect determinations is thus a sensitive probe for the presence of non-SM particles in quark transitions. The current world average of direct measurements is $(66.4_{-3.0}^{+2.8})^\circ$ [5], dominated by results from the LHCb collaboration [6]. From indirect determinations, the CKMfitter group obtains $\phi_3 = (66.29_{-1.86}^{+0.72})^\circ$ [7], while the UT_{fit} Collaboration finds $(65.2 \pm 1.5)^\circ$ [8]. The difference in precision between direct and indirect determinations implies that an improvement in the former is important to better constrain non-SM contributions to CP violation.

¹Throughout this paper, charge-conjugation is implied unless stated otherwise.

The angle ϕ_3 is determined directly from the analysis of $B^+ \rightarrow Dh^+$ decays, where D is an admixture of D^0 and \bar{D}^0 flavour eigenstates and h is a kaon or pion. The interference between the favoured $B^+ \rightarrow \bar{D}^0 h^+$ decay amplitude mediated by a $b \rightarrow c$ transition, \mathcal{A}_{fav} , and the suppressed $B^+ \rightarrow D^0 h^+$ decay amplitude mediated by a $b \rightarrow u$ transition, \mathcal{A}_{sup} , depends on ϕ_3 and two hadronic parameters r_B^X and δ_B^X , which are given by the relation

$$\mathcal{A}_{\text{sup}}/\mathcal{A}_{\text{fav}} = r_B^X e^{i(\delta_B^X + \phi_3)}, \quad (1.1)$$

where r_B and δ_B represent the decay-amplitude ratio and difference in strong-interaction phase between the suppressed and favoured mode, respectively, and X is the B final state. For $B^- \rightarrow Dh^-$ decays, the sign of ϕ_3 is flipped. Equation 1.1 implies that the sensitivity to ϕ_3 is approximately inversely proportional to the value of r_B^X , which is around 0.1 for $B^+ \rightarrow DK^+$ decays and 0.005 for $B^+ \rightarrow D\pi^+$ decays [9]. Hence, the sensitivity to ϕ_3 in $B^+ \rightarrow D\pi^+$ decays is considerably worse than that in $B^+ \rightarrow DK^+$ decays, despite larger signal yields.

This paper presents a determination of ϕ_3 from a combination of measurements using samples of up to 711 fb^{-1} from the Belle experiment and up to 362 fb^{-1} from the Belle II experiment using inputs from $B^+ \rightarrow DK^+$, $B^+ \rightarrow D\pi^+$, and $B^+ \rightarrow D^*(\rightarrow D\pi^0, D\gamma)K^+$ decays. We use the values and correlations, when available, of the observables reported for these decays as inputs, incorporating them into a likelihood based on their relationships with ϕ_3 and the hadronic parameters. The angle ϕ_3 and the hadronic parameters are obtained by maximizing the likelihood and using a frequentist technique based on the Feldman-Cousins method [10] for the construction of confidence regions. The impact of assumptions on the unknown correlations and the relative contributions of each input to the final results are discussed. The rest of the paper is organized as follows. Section 2 describes the ϕ_3 extraction methods for the final states used in this combination. In Section 3, we present the Belle and Belle II results entering the combination, and we list the necessary additional inputs in Section 4. Section 5 briefly outlines the statistical treatment. In Section 6, we show the results and discuss their interpretation. A summary is presented in Section 7.

2 Methods to obtain ϕ_3

We use four methods that directly determine ϕ_3 . We provide a brief overview of each, illustrating the relevant observables in Section 3, and details of their dependences on ϕ_3 , $r_B^{D^{(*)}h}$, and $\delta_B^{D^{(*)}h}$ in Appendix C.

The Gronau-London-Wyler (GLW) method uses the decays of D mesons to CP eigenstates, such as the CP -even ($CP+$) decay $D \rightarrow K^- K^+$ and the CP -odd ($CP-$) decay $D \rightarrow K_S^0 \pi^0$ [11, 12]. The Atwood-Dunietz-Soni (ADS) method uses final states, such as $D \rightarrow K^\pm \pi^\mp$, in which the interference between suppressed B decay followed by the Cabibbo-allowed D decay with the favoured B decay followed by the doubly Cabibbo-suppressed D decay generate large CP asymmetries [13, 14]. In this method, an additional dependence on the properties of the D decay is introduced through the ratio of suppressed and favoured D decay amplitudes, r_D , and their strong-interaction phase difference, δ_D .

The ADS method has been extended to multibody D decays, such as $D \rightarrow K^+\pi^-\pi^0$, where an extra coherence factor κ_D is introduced to account for the dilution from the inseparable multiple interfering amplitudes integrated over the D -decay phase space (Dalitz plot) [15]. All these parameters are measured independently and are auxiliary inputs in our combination.

The relevant physics observables are CP -violating decay-rate asymmetries,

$$A_f = \frac{\mathcal{B}(B^- \rightarrow D_f K^-) - \mathcal{B}(B^+ \rightarrow D_{\bar{f}} K^+)}{\mathcal{B}(B^- \rightarrow D_f K^-) + \mathcal{B}(B^+ \rightarrow D_{\bar{f}} K^+)}, \quad (2.1)$$

and CP -averaged decay-rate ratios,

$$R_f = \frac{\mathcal{B}(B^- \rightarrow D_f K^-) + \mathcal{B}(B^+ \rightarrow D_{\bar{f}} K^+)}{\mathcal{B}(B^- \rightarrow D_{\bar{f}} h^-) + \mathcal{B}(B^+ \rightarrow D_f h^+)}, \quad (2.2)$$

where f indicates that the D meson is reconstructed in a CP eigenstate (noneigenstate) and h is a pion (kaon) and \bar{f} indicates the same CP (flavour conjugate) final state for the GLW (ADS) measurements. The double ratio, for the GLW measurements, is defined as

$$\mathcal{R}_{CP\pm} \approx \frac{R_{CP\pm}}{R_{\text{flav}}}, \quad (2.3)$$

where $R_{CP\pm}$ or R_{flav} results from specializing Equation 2.2 for a $CP\pm$ or flavour-specific final state, respectively. The use of double ratios helps to reduce the systematic uncertainties from branching fractions and reconstruction efficiencies of different D channels appearing in the numerator and denominator of Equation 2.2. Equation 2.3 is exact in the limit at which the Cabibbo-suppressed contributions to the $B^- \rightarrow D_f \pi^-$ decay amplitudes completely vanish, as detailed in Ref. [16]. These asymmetries and ratios are directly related to ϕ_3 and other parameters through terms proportional to $\sin \delta \sin \phi_3$ and $\cos \delta \cos \phi_3$, respectively, as described in Appendix C.

The Grossman-Ligeti-Soffer (GLS) method exploits singly Cabibbo-suppressed decays $D \rightarrow K_s^0 K^\pm \pi^\mp$ [17]. These two different processes are labeled as “same-sign (SS)” and “opposite-sign (OS)”, according to the relationship between the charges of the parent B meson and the K meson from the D decay. The observables include CP asymmetries of $B^+ \rightarrow DK^+$ and $B^+ \rightarrow D\pi^+$ decays for each process, the CP -averaged ratio of the $B^+ \rightarrow DK^+$ branching-fraction relative to that of $B^+ \rightarrow D\pi^+$ for each process, and an additional ratio of the SS branching-fraction relative to that of OS for $B^+ \rightarrow D\pi^+$. This method requires information about the properties of the D decay, which is encapsulated in the values of r_D , δ_D , and κ_D , included as auxiliary external inputs in our combination.

The Bondar-Poluektov-Giri-Grossman-Soffer-Zupan (BPGGSZ) method relies on self-conjugate multibody- D -meson decays such as $K_s^0 h^- h^+$. This method uses two approaches, which are either dependent [18] or independent [19, 20] of the modelling of the $D \rightarrow K_s^0 h^- h^+$ decay amplitude. The model-dependent approach relies upon a detailed description of the intermediate-resonance structure of the D -decay amplitude and nonresonant contributions. The model-independent method exploits CP -asymmetry measurements in disjoint regions (bins) of the Dalitz plot that can be related to ϕ_3 using model-independent

measurements of D -decay strong-interaction-phase parameters. The population of candidates in the Dalitz plot depends on four variables,

$$x_{\pm}^X = r_B^X \cos(\delta_B^X \pm \phi_3), \quad (2.4)$$

$$y_{\pm}^X = r_B^X \sin(\delta_B^X \pm \phi_3). \quad (2.5)$$

The $D \rightarrow K_s^0 h^- h^+$ decay proceeds via several intermediate resonances, which results in a variation of the CP asymmetry over the Dalitz plot, providing the best sensitivity to ϕ_3 among all the methods.

Subleading effects from $D^0 - \bar{D}^0$ mixing can impact the determination of ϕ_3 [21]. They are accounted for in this combination only for the ADS channels, where $D^0 - \bar{D}^0$ mixing contributes at leading order in the relations between ϕ_3 , other parameters, and the ADS observables R_{ADS} and A_{ADS} (see Ref. [21] and Equations C.4 in Appendix C). The magnitude of the effect is inversely proportional to r_B^X , making it particularly significant for $B^+ \rightarrow D\pi^+$ decays. For consistency, $D^0 - \bar{D}^0$ mixing effects are also included for $B^+ \rightarrow DK^+$ modes. The contribution from $D^0 - \bar{D}^0$ mixing cancels in the CP asymmetries and is negligible in the ratios of the GLW observables. Charm mixing is ignored in the BPGGSZ result, as to properly account for it a new measurement would be required taking into account its effects in the determination of the D -decay strong-interaction-phase parameters. However, the bias from neglecting charm mixing in BPGGSZ channels is estimated to be less than 0.2° [21], i.e., negligible compared to the expected precision of this combination. Due to the limited precision, $D^0 - \bar{D}^0$ mixing is also neglected in the GLS results. Finally, we ignore the small effect of direct CP violation in D decays [22].

3 Inputs from Belle and Belle II analyses

We summarize the measurements used as inputs in our combination in Table 1 and briefly describe them below. The values of the observables with their uncertainties and correlations are provided in Appendix D.

Table 1. Belle and Belle II measurements used for the combination, m.i. and m.d. stand for model-independent and model-dependent, respectively.

B decay	D decay	Method	Data set (Belle + Belle II)[fb $^{-1}$]	Ref.
$B^+ \rightarrow Dh^+$	$D \rightarrow K_s^0 \pi^0, K^- K^+$	GLW	711 + 189	[23]
$B^+ \rightarrow Dh^+$	$D \rightarrow K^+ \pi^-, K^+ \pi^- \pi^0$	ADS	711 + 0	[15, 24]
$B^+ \rightarrow Dh^+$	$D \rightarrow K_s^0 K^- \pi^+$	GLS	711 + 362	[25]
$B^+ \rightarrow Dh^+$	$D \rightarrow K_s^0 h^- h^+$	BPGGSZ (m.i.)	711 + 128	[26]
$B^+ \rightarrow Dh^+$	$D \rightarrow K_s^0 \pi^- \pi^+ \pi^0$	BPGGSZ (m.i.)	711 + 0	[27]
$B^+ \rightarrow D^* K^+$	$D^* \rightarrow D\pi^0, D \rightarrow K_s^0 \pi^0, K_s^0 \phi, K_s^0 \omega,$ $K^- K^+, \pi^- \pi^+$	GLW	210+0	[12]
$B^+ \rightarrow D^* K^+$	$D^* \rightarrow D\pi^0, D\gamma, D \rightarrow K_s^0 \pi^- \pi^+$	BPGGSZ (m.d.)	605 + 0	[28]

- $B^+ \rightarrow Dh^+, D \rightarrow K_S^0 \pi^0, K^- K^+$. This GLW measurement is based on the combined $(711 + 189) \text{ fb}^{-1}$ Belle and Belle II data sets, and provides two CP asymmetries and two CP -averaged ratios, defined in Equations 2.1 and 2.3, obtained from a simultaneous fit to $B^+ \rightarrow Dh^+$ decays [23].
- $B^+ \rightarrow Dh^+, D \rightarrow K^+ \pi^-, K^+ \pi^- \pi^0$. These ADS measurements are based on the full 711 fb^{-1} Belle data set. They provide observables, such as CP asymmetry and CP -averaged ratio from each channel, defined in Equations 2.1 and 2.2 [15, 24].
- $B^+ \rightarrow Dh^+, D \rightarrow K_S^0 K^- \pi^+$. This GLS measurement is based on the combined Belle and Belle II data samples, $(711 + 362) \text{ fb}^{-1}$ and provides four CP asymmetries and three branching-fraction ratios as inputs to the combination, defined in Equations C.8. We use only the results restricted to the quasi-two-body $D \rightarrow K^\pm K^{*\mp}$ region as the resulting enhanced interference improves the expected precision [25].
- $B^+ \rightarrow Dh^+, D \rightarrow K_S^0 h^- h^+$. This is a model-independent BPGGSZ measurement based on a combination of Belle and Belle II data sets corresponding to $(711 + 128) \text{ fb}^{-1}$ of integrated luminosity [26]. The variables, defined in Equations 2.4 and 2.5, are obtained from a simultaneous fit to the Dalitz plots of $D \rightarrow K_S^0 h^- h^+$ decays. In this measurement, a parametrization was adopted, which exploits the common dependence on ϕ_3 in $B^+ \rightarrow DK^+$ and $B^+ \rightarrow D\pi^+$ decays by introducing a single complex variable [29, 30]

$$\xi^{D\pi} = \left(\frac{r_B^{D\pi}}{r_B^{DK}} \right) e^{i(\delta_B^{D\pi} - \delta_B^{DK})}. \quad (3.1)$$

The resulting input observables for $B^+ \rightarrow D\pi^+$ decays are defined as $x_\xi^{D\pi} \equiv \text{Re}(\xi^{D\pi})$ and $y_\xi^{D\pi} \equiv \text{Im}(\xi^{D\pi})$. The analogous observables, for $B^+ \rightarrow DK^+$ decays defined in Equations 2.4 and 2.5, are written in terms of $B^+ \rightarrow DK^+$ observables as

$$x_\pm^{D\pi} = x_\xi^{D\pi} x_\pm^{DK} - y_\xi^{D\pi} y_\pm^{DK}, \quad y_\pm^{D\pi} = x_\xi^{D\pi} y_\pm^{DK} + y_\xi^{D\pi} x_\pm^{DK}. \quad (3.2)$$

Hence, this measurement provides the following six input observables for the combination: $x_\pm^{DK}, y_\pm^{DK}, x_\xi^{D\pi}$, and $y_\xi^{D\pi}$.

- $B^+ \rightarrow Dh^+, D \rightarrow K_S^0 \pi^- \pi^+ \pi^0$. This is a model-independent BPGGSZ measurement performed on the full Belle data set, corresponding to an integrated luminosity of 711 fb^{-1} [27]. The variables, defined in Equations 2.4 and 2.5, are obtained using a fit to the Dalitz plot of $D \rightarrow K_S^0 \pi^- \pi^+ \pi^0$ decays.
- $B^+ \rightarrow D^* K^+, D^* \rightarrow D\pi^0, D \rightarrow K_S^0 \pi^0, K_S^0 \phi, K_S^0 \omega, K^- K^+, \pi^- \pi^+$. This GLW measurement is based on a 210 fb^{-1} subset of Belle data [12]. The input observables are defined in Equations 2.1 and 2.3.
- $B^+ \rightarrow D^* K^+, D^* \rightarrow D\pi^0, D\gamma, D \rightarrow K_S^0 \pi^- \pi^+$. This is a model-dependent BPGGSZ measurement based on a 605 fb^{-1} subset of Belle data [28]. The input observables are defined in Equations 2.4 and 2.5.

We do not use inputs from $B^0 \rightarrow D^{(*)}h^{(*)}$ decays [31–33] in the combination because, due to their limited precision and their dependence on additional external parameters, they would have negligible impact on the determination of ϕ_3 .

4 Auxiliary inputs

Several auxiliary inputs are needed to constrain the D -decay parameters to extract ϕ_3 . These are summarized in Table 2 and briefly described below. Correlations between inputs are reported in Appendix E.

Table 2. Auxiliary input observables and their values used in the ϕ_3 combination.

Decay	Observable	Value	Source	Reference
$D \rightarrow K^+\pi^-$	$R_D^{K\pi}$	$(3.44 \pm 0.02) \times 10^{-3}$	HFLAV	[9]
	$\delta_D^{K\pi}$	$(191.7 \pm 3.7)^\circ$		
	$r_D^{K\pi} \cos(\delta_D^{K\pi})$	-0.0562 ± 0.0081	BESIII	[34]
$r_D^{K\pi} \sin(\delta_D^{K\pi})$	-0.011 ± 0.012			
$D \rightarrow K^+\pi^-\pi^0$	$r_D^{K\pi\pi^0}$	0.0441 ± 0.0011	CLEO + LHCb + BESIII	[35]
	$\kappa_D^{K\pi\pi^0}$	0.79 ± 0.04		
	$\delta_D^{K\pi\pi^0}$	$(196 \pm 11)^\circ$		
$D^0 - \bar{D}^0$ mixing	x_D	$(0.407 \pm 0.044)\%$	HFLAV	[9]
	y_D	$(0.647 \pm 0.024)\%$		
$D \rightarrow K_S^0 K^- \pi^+$	$(r_D^{K_S^0 K\pi})^2$	0.356 ± 0.034	CLEO	[36]
	$\kappa_D^{K_S^0 K\pi}$	0.94 ± 0.12		
	$\delta_D^{K_S^0 K\pi}$	$(-16.6 \pm 18.4)^\circ$		
	$(r_D^{K_S^0 \bar{K}\pi})^2$	0.370 ± 0.003	LHCb	[37]
$B^+ \rightarrow Dh^+$	R_{GLS}	0.0789 ± 0.0027	PDG	[5]

- **Input for $D \rightarrow K^+\pi^-$ decays.** The ADS measurement requires the ratio $r_D^{K\pi}$ and strong-interaction phase difference $\delta_D^{K\pi}$ between favoured $D \rightarrow K^-\pi^+$ and suppressed $D \rightarrow K^+\pi^-$ decays to constrain the properties of the charm system. We take these from the HFLAV global fit to measurements of CP -violation and mixing in the $D^0 - \bar{D}^0$ system [9]. The value of $\delta_D^{K\pi}$ is shifted by 180° compared to Ref. [9] to match the phase convention adopted in this work. The parameter $R_D^{K\pi}$ is the square of the amplitude ratio $r_D^{K\pi}$. We also include a measurement from BESIII [34] performed on a $2.93 \text{ fb}^{-1} \psi(3770)$ data set, which is not included in Ref. [9].
- **Input for $D \rightarrow K^+\pi^-\pi^0$ decays.** The ADS measurement with $D \rightarrow K^+\pi^-\pi^0$ decays requires knowledge of hadronic parameters describing the D decay. These are the amplitude ratio $r_D^{K\pi\pi^0}$, strong-interaction phase difference $\delta_D^{K\pi\pi^0}$, and coherence factor $\kappa_D^{K\pi\pi^0}$. We take the combined result of BESIII, CLEO, and LHCb from Ref. [35].

- **$D^0 - \bar{D}^0$ mixing parameters.** The ADS measurements require the charm mixing parameters x_D and y_D as inputs. We obtain these inputs from the HFLAV global fit to measurements of CP -violation and mixing in the $D^0 - \bar{D}^0$ system [9]. The HFLAV average of x_D is dominated by the LHCb measurement of Ref. [38], which uses as input the same D -decay strong-interaction-phase parameters as used in our BPGGSZ result. The correlation introduced by these common inputs is neglected in this combination, as the impact of the D -decay strong-interaction-phase parameters in the BPGGSZ result is small compared to the precision of the measurement [26].
- **Input for $D \rightarrow K_S^0 K^- \pi^+$ decays.** The GLS measurement with $D \rightarrow K_S^0 K^- \pi^+$ decays requires the hadronic parameters $r_D^{K_S^0 K \pi}$, $\delta_D^{K_S^0 K \pi}$, and $\kappa_D^{K_S^0 K \pi}$. We use the measurement from CLEO [36] and the $r_D^{K_S^0 K \pi}$ result from LHCb [37]. In addition, we take the ratio of branching fractions $R_{\text{GLS}} = \mathcal{B}(B^- \rightarrow D^0 K^-) / \mathcal{B}(B^- \rightarrow D^0 \pi^-)$ from Ref. [5].

5 Statistical treatment

We determine ϕ_3 and six hadronic parameters r_B^{DK} , δ_B^{DK} , $r_B^{D\pi}$, $\delta_B^{D\pi}$, $r_B^{D^*K}$, and $\delta_B^{D^*K}$ using the relations defined in Equations C.1, C.4, C.6, and C.8. These relations require values of eight D -decay parameters and one B -decay ratio, summarized in Section 4. We combine all auxiliary inputs and results from Belle and Belle II measurements in a maximum-likelihood fit.

We denote the set of all experimental observables as \vec{X} and underlying physics parameters including ϕ_3 as $\vec{\theta}$. For a particular set of observables, \vec{X}^{obs} , the likelihood function is defined as the product of the probability density functions (PDFs),

$$\mathcal{L}(\vec{\theta} | \vec{X}^{\text{obs}}) = \prod_i f_i(\vec{X}_i^{\text{obs}} | \vec{\theta}), \quad (5.1)$$

where $f_i(\vec{X}_i^{\text{obs}} | \vec{\theta})$ is the PDF of observables \vec{X}_i^{obs} for each measurement i . For each of the inputs, we assume the observables follow Gaussian distributions

$$f_i(\vec{X}_i^{\text{obs}} | \vec{\theta}) \propto \exp \left\{ -\frac{1}{2} [\vec{X}_i(\vec{\theta}) - \vec{X}_i^{\text{obs}}]^T V_i^{-1} [\vec{X}_i(\vec{\theta}) - \vec{X}_i^{\text{obs}}] \right\}, \quad (5.2)$$

where V_i^{-1} is the experimental covariance matrix, which accounts for statistical and systematic uncertainties and their correlations. The correlation of systematic uncertainties within an experiment is ignored. For the case where the uncertainties are asymmetric, we symmetrize them, without changing the central value, by substituting the standard deviation of the distribution observed in simulated experiments generated using the asymmetric Gaussian likelihood function. We estimate $\vec{\theta}$ by minimizing a χ^2 -like quantity defined as $\chi^2(\vec{\theta} | \vec{X}^{\text{obs}}) = -2 \ln \mathcal{L}(\vec{\theta} | \vec{X}^{\text{obs}})$. The best-fit value is given by the global minimum of the χ^2 function, $\chi^2(\vec{\theta}_{\text{min}})$.

To estimate the confidence level (CL) for each parameter, we use the test statistic defined as $\Delta\chi^2 = \chi^2(\vec{\theta}_{\text{min}}^{\dagger}) - \chi^2(\vec{\theta}_{\text{min}})$, where $\chi^2(\vec{\theta}_{\text{min}}^{\dagger})$ is the χ^2 function at the $\vec{\theta}_{\text{min}}^{\dagger}$ value

of the parameter. We generate simulated experiments with parameters $\vec{\theta}$ set to $\vec{\theta}'_{\min}$ and calculate $\Delta\chi^{2'}$ by replacing \vec{X}_{obs} with the simulated experiments and minimising with respect to $\vec{\theta}$. The value of $1 - \text{CL}$ is calculated as the fraction of the simulated experiments that have larger $\Delta\chi^{2'}$ ($\Delta\chi^2 < \Delta\chi^{2'}$) than the measured data. This approach is known as the `PLUGIN` method.

6 Results

We combine 59 input observables from the measurements listed in Tables 1 and 2 to determine ϕ_3 and the six B -decay hadronic parameters $r_B^{D^{(*)}h}$ and $\delta_B^{D^{(*)}h}$. The fit has a total of 18 free parameters, including eight D -decay hadronic parameters. We obtain $\phi_3 = (75.2^{+7.1}_{-7.5})^\circ$, where the uncertainties include the statistical and systematic contributions from all inputs. The results for other parameters are summarized in Table 3, where we report central values and confidence intervals at 68.3% and 95.4% probability. We show the χ^2 values for each measurement in Appendix A. We also show the pull distribution in Appendix B, which is defined as $(A_{\text{obs}} - A_{\text{fit}})/\sigma(\text{obs})$, where A_{obs} and A_{fit} are the input value and the best-fit value, respectively, and $\sigma(\text{obs})$ is the measurement uncertainty. Table 4 gives the combined statistical and systematic correlation matrix for these parameters. The goodness of the fit calculated from the fraction of simulated experiments, generated from the best-fit point, which have a χ^2 larger than that found in the data is $p = (55.4 \pm 0.2)\%$. We perform a one-dimensional profile-likelihood scan for ϕ_3 , the strong-interaction phase $\delta_B^{D^{(*)}h}$, and the amplitude ratio $r_B^{D^{(*)}h}$. Figure 1 shows the $1 - \text{CL}$ distributions as function of the scanned parameters. We also perform the two-dimensional profile-likelihood scan for $(\phi_3, r_B^{D^{(*)}h})$ and $(\phi_3, \delta_B^{D^{(*)}h})$. The corresponding confidence regions are shown in Figure 2.

Table 3. Combination results: best-fit values and 68.3% and 95.4% confidence intervals.

Parameters	$\phi_3(^\circ)$	r_B^{DK}	$\delta_B^{DK}(^\circ)$	$r_B^{D\pi}$	$\delta_B^{D\pi}(^\circ)$	$r_B^{D^*K}$	$\delta_B^{D^*K}(^\circ)$
Best-fit value	75.2	0.115	137.8	0.0165	347.0	0.229	342
68.3% interval	[67.7, 82.3]	[0.102, 0.127]	[128.0, 146.3]	[0.0113, 0.0220]	[337.4, 355.7]	[0.162, 0.297]	[326, 356]
95.4% interval	[59, 89]	[0.089, 0.138]	[116, 154]	[0.006, 0.027]	[322, 366]	[0.10, 0.37]	[306, 371]

We also investigate the individual contributions of each method by presenting two-dimensional confidence regions for various configurations of combinations that include only subsets of inputs, as shown in Figure 3. The 68.3% confidence intervals for these are listed in Table 5. As expected, the sensitivity is mostly dominated by the BPGGSZ measurements. Following closely are inputs from the ADS-like final states, with the GLW measurements and other results being the next most significant. We do not report the individual contributions of the ADS and GLW inputs, as they are strongly correlated with nuisance parameters obtained from the predominant BPGGSZ measurements in this combination. A comprehensive discussion of this effect can be found below.

A proper combination should include the statistical and systematic correlations between inputs. However, correlations between input observables are not available for all

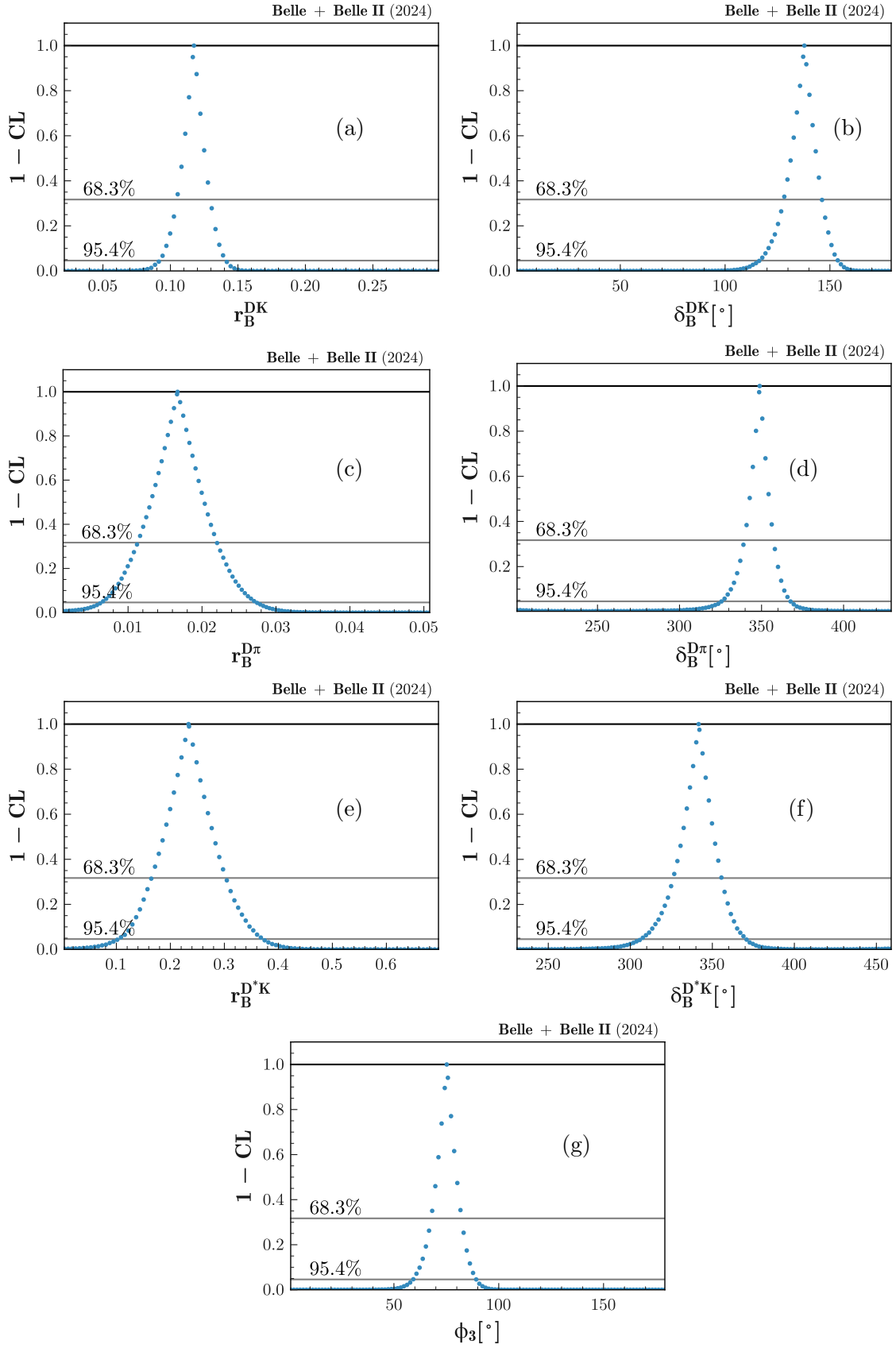


Figure 1. 1 - CL distributions as functions of (a) r_B^{DK} , (b) δ_B^{DK} , (c) $r_B^{D\pi}$, (d) $\delta_B^{D\pi}$, (e) $r_B^{DK^*}$, (f) $\delta_B^{DK^*}$, and (g) ϕ_3 .

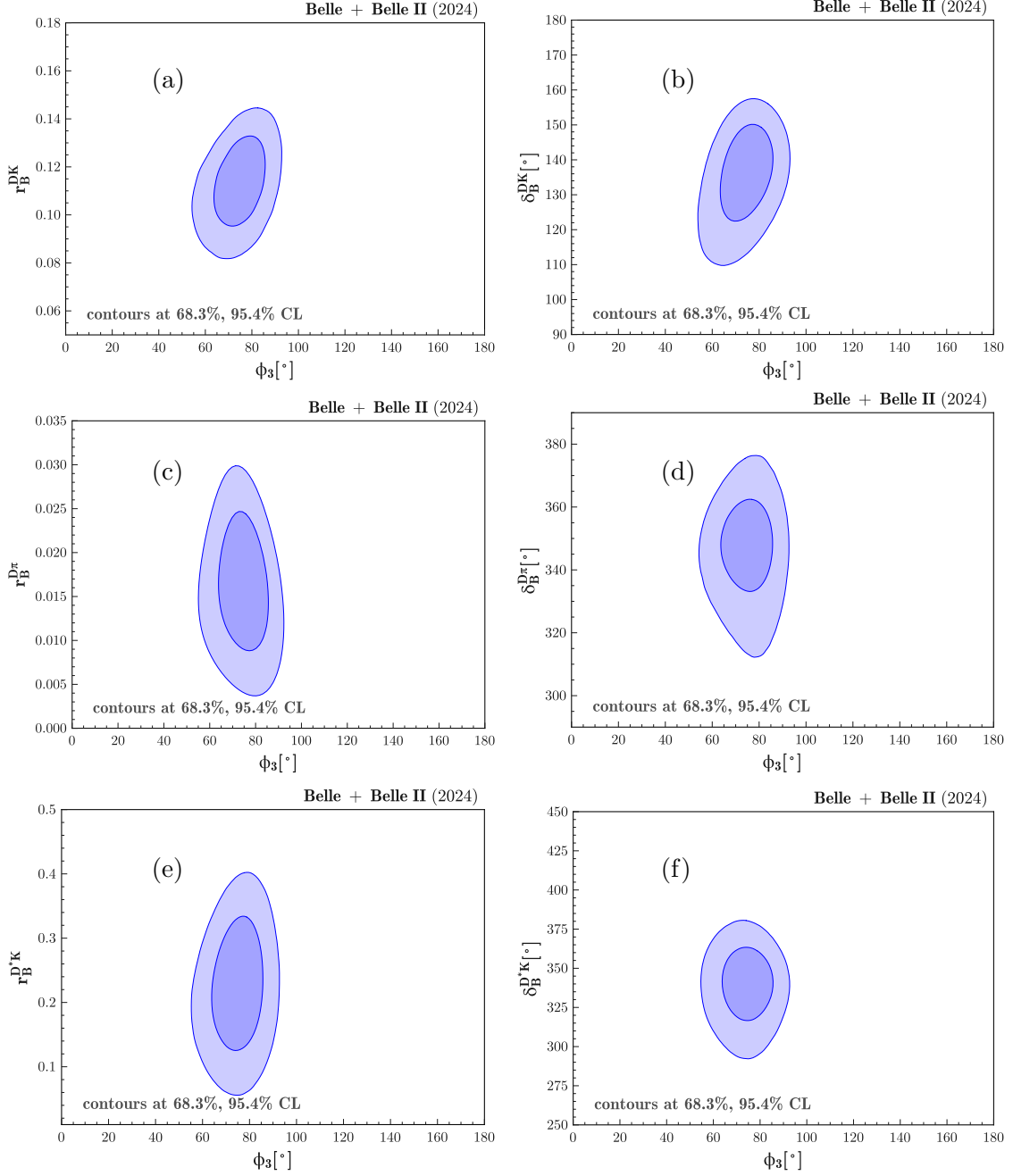


Figure 2. Two-dimensional confidence regions at the (inner curve) 68.3% and (outer curve) 95.4% confidence levels, obtained for (a) $r_B^{DK} - \phi_3$, (b) $\delta_B^{DK} - \phi_3$, (c) $r_B^{D\pi} - \phi_3$, (d) $\delta_B^{D\pi} - \phi_3$, (e) $r_B^{D^*K} - \phi_3$, and (f) $\delta_B^{D^*K} - \phi_3$.

Table 4. Combined statistical and systematic correlations between ϕ_3 and hadronic parameters.

	ϕ_3	r_B^{DK}	δ_B^{DK}	$r_B^{D\pi}$	$\delta_B^{D\pi}$	$r_B^{D^*K}$	$\delta_B^{D^*K}$
ϕ_3	1.000	0.364	0.325	-0.158	0.005	0.155	-0.016
r_B^{DK}		1.000	0.256	0.054	0.012	0.056	-0.006
δ_B^{DK}			1.000	0.111	0.105	0.050	-0.005
$r_B^{D\pi}$				1.000	0.146	-0.025	0.003
$\delta_B^{D\pi}$					1.000	0.000	0.000
$\delta_B^{D\pi}$					1.000	0.000	0.000
$r_B^{D^*K}$						1.000	0.168
$\delta_B^{D^*K}$							1.000

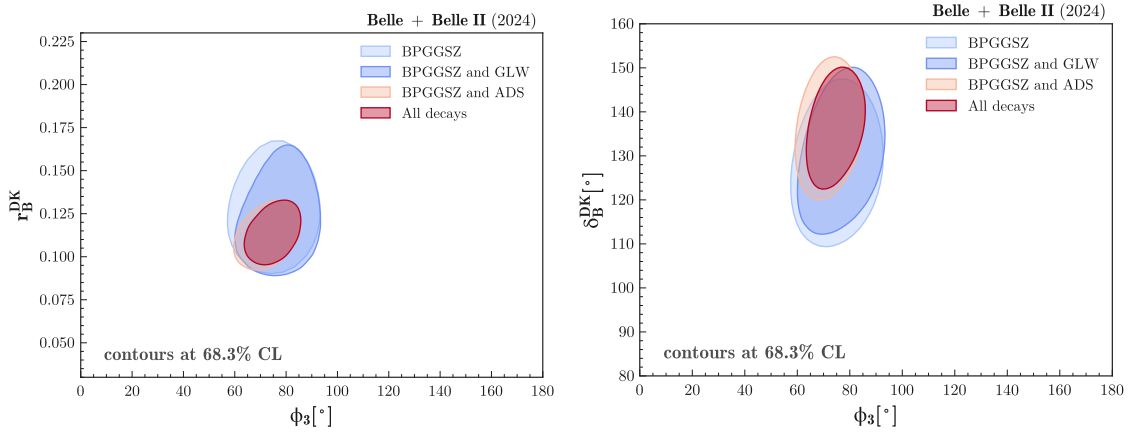


Figure 3. Two-dimensional confidence regions at the 68.3% confidence levels, combining measurements based on various methods, for $r_B^{DK} - \phi_3$ (left) and $\delta_B^{DK} - \phi_3$ (right).

Table 5. One-dimensional confidence intervals at the 68.3% probability, derived from the combination of measurements from various methods. Additional uncertainties due to assumptions on the unknown correlations are not included in these intervals.

Method	BPGGSZ	BPGGSZ and GLW	BPGGSZ and ADS
$\phi_3(^{\circ})$	[65, 87]	[68, 90]	[64.2, 80.8]
r_B^{DK}	[0.104, 0.156]	[0.098, 0.146]	[0.100, 0.126]
$\delta_B^{DK}(^{\circ})$	[118, 142]	[117, 143]	[126, 148]
$r_B^{D\pi}$	[0.0111, 0.0235]	[0.0117, 0.0237]	[0.0118, 0.0223]
$\delta_B^{D\pi}(^{\circ})$	[317, 355]	[323, 357]	[337.4, 355.4]

modes. For example, statistical correlations are not given for Refs. [12] and [15] and systematic correlations are not provided by Refs. [12], [15], [24], [27], and [28]. Our choice is to set the unknown correlations to zero in the central combination and assign an additional uncertainty to the results due to this assumption. To calculate the additional uncertainty, we set the unknown statistical correlations to ± 0.3 and monitor the changes in results

when varying the unknown systematic correlations up to ± 0.9 . The choice of the value ± 0.3 is based on knowledge of known correlations in other ADS and GLW-like final states, as reported in Refs. [23] and [24], respectively. We examine the results when correlations are changed individually and collectively and assign the largest difference observed on the ϕ_3 central values with respect to the nominal result as an additional uncertainty. For ϕ_3 , this is $(^{+2.8}_{-1.3})^\circ$. This additional uncertainty is added in quadrature to the result in Table 3, giving the final result of $\phi_3 = (75.2 \pm 7.6)^\circ$. The additional uncertainties for other parameters are negligible compared to the nominal uncertainties, as shown in Table 6. We ignore the correlation of systematic uncertainties between different measurements from the same experiments. As the precision of these measurements is dominated by statistical uncertainties, the impact of neglecting such correlations is negligible.

Table 6. Additional uncertainties on all the parameters due to unknown correlations.

Parameters	$\phi_3(^\circ)$	r_B^{DK}	$\delta_B^{DK}(^\circ)$	$r_B^{D\pi}$	$\delta_B^{D\pi}(^\circ)$	$r_B^{D^*K}$	$\delta_B^{D^*K}(^\circ)$
Uncertainty	$+2.8$ -1.3	$+0.005$ -0.005	$+1.7$ -0.7	$+0.0001$ -0.001	$+0$ -0.7	$+0.002$ -0	$+0.2$ -0.1

6.1 Discussion

Our combined determination of ϕ_3 alone is consistent with the current world average value within two standard deviations (σ) [9]. However, the collective agreement of our full set of results with the world average values is poor, with a p -value of 0.45%.² In addition, the sensitivity obtained for ϕ_3 is better than originally anticipated [39].

The discrepancy with the world average arises primarily from the large values obtained for $r_B^{D\pi}$ and $\delta_B^{D\pi}$, which deviate by 2.2σ and 4.0σ , respectively, from the world average values.³ These parameters are correlated: a large $r_B^{D\pi}$ value results in a smaller uncertainty on $\delta_B^{D\pi}$, thus giving a larger deviation for this parameter. The large $r_B^{D\pi}$ value is mainly determined by the values of input observables in Equation 3.1. While these observables agree within 2σ with the values reported by the only other measurement available with this parametrization [40], their large central values lead to an unexpectedly high $r_B^{D\pi}$ value. For instance, the expected value for the $r_B^{D\pi}/r_B^{DK}$ ratio is approximately 1/20, considering only the ratio of CKM matrix-elements involved in the amplitudes, i.e., $|V_{ub}^*V_{cd}/V_{cb}^*V_{ud}|$. However, we obtain approximately 1/7 for this ratio in our combination. We demonstrate that the departure of our results from the world averages is due to our higher measured value of $r_B^{D\pi}$ by repeating the combination after constraining $r_B^{D\pi}$ to its expected value $r_B^{D\pi} = 0.0053 \pm 0.0007$, estimated using the known branching fractions of various $B \rightarrow DK$ and $B \rightarrow D\pi$ decays and SU(3) symmetry [41]. With this additional constraint, our combined ϕ_3 value is $(78.7 \pm 8.1)^\circ$, which is not significantly different from the nominal

²In the comparison, we do not include the correlation due to the common Belle results used in our combination and in the current world average.

³In this context, the ‘‘world average’’ refers to the LHCb average of $r_B^{D\pi}$ and $\delta_B^{D\pi}$, as there are currently no world average values for $r_B^{D\pi}$ and $\delta_B^{D\pi}$ [9].

result. However, the resulting increased uncertainty on $\delta_B^{D\pi}$ yields better agreement of the full set of results with the world averages, with a p -value of 13%.

The second aspect that requires further checks is our better-than-expected sensitivity to ϕ_3 [39]. We investigate this by studying separately the contribution of the individual inputs to the ϕ_3 precision, as shown in Table 5. The precision on ϕ_3 improves significantly, from 11° to 8.3° , when the ADS inputs from $B^+ \rightarrow D(\rightarrow K^+\pi^-)h^+$ are combined with the BPGGSZ inputs. This enhancement is driven by the R_{ADS} observable of the $B^+ \rightarrow D\pi^+$ channel. The relation of this observable with hadronic parameters in the absence of $D^0 - \bar{D}^0$ mixing is

$$R_{\text{ADS}}^{D\pi, K\pi} = (r_B^{D\pi})^2 + (r_D^{K\pi})^2 + 2r_B^{D\pi}r_D^{K\pi} \cos(\delta_B^{D\pi} + \delta_D^{K\pi}) \cos \phi_3. \quad (6.1)$$

Substitution in the above equation of our $r_B^{D\pi}$ value, the auxiliary input $r_D^{K\pi}$, and their uncertainties, greatly enhances the precision on the interference (last) term as compared to the $B^+ \rightarrow DK^+$ case. Furthermore, our value $\delta_B^{D\pi} \approx 347^\circ$ leads to a precise determination of $\cos(\delta_B^{D\pi} + \delta_D^{K\pi})$ close to one. The combined effect of both factors improves the precision of our ϕ_3 result. The ADS contribution to the sensitivity of ϕ_3 is primarily attributed to three elements: the small relative uncertainty of the large $r_B^{D\pi}$ value favoured by Belle and Belle II measurements, the availability of a precise value of $r_D^{K\pi}$ from global averages, and the large $\delta_B^{D\pi}$ value favoured by Belle and Belle II measurements.

Finally, we check the impact of our large r_B^{DK} value, which is 1.5σ higher than the world average. We generate simulated experiments assuming world average values for ϕ_3 and of the hadronic parameters. Repeating the analysis on these gives 12° precision on ϕ_3 . We repeat the study assuming our combined value for r_B^{DK} and observe that the precision improves to 10.1° . Finally, we repeat the study by assuming our combined values for $\phi_3, r_B^{DK}, \delta_B^{DK}, r_B^{D\pi}$, and $\delta_B^{D\pi}$ and obtain a precision of 7.1° , which is consistent with our nominal results.

By employing simulated experiments generated using world average values, we extrapolate this result to future sample sizes, and find the current uncertainty on ϕ_3 to be consistent with recent projections [39].

6.2 Coverage study

We check the statistical coverage of the fit by generating simulated experiments at the best-fit point. The coverage is then defined as the fraction of times the 1σ or 2σ interval of the fitted ϕ_3 contains the true value of ϕ_3 . We perform the coverage study assuming that the true values of all relevant parameters are the values measured in our data. The resulting fractions are 0.672 ± 0.004 and 0.951 ± 0.002 for 1σ and 2σ coverage, respectively.

We also test coverage at $r_B^{DK, D\pi}$ values other than the best-fit point; the 1σ and 2σ coverage is shown in Figure 4. The coverage for the combination degrades as the true values of $r_B^{DK, D\pi}$ become smaller. This behaviour has previously been observed by the CKMfitter group [7] and the LHCb experiment [42]. The fitted values found in this combination, $r_B^{DK} = 0.115$ and $r_B^{D\pi} = 0.016$, are well within the regime of accurate coverage. No correction for under-coverage is applied to the confidence intervals quoted in Tables 3 and 5.

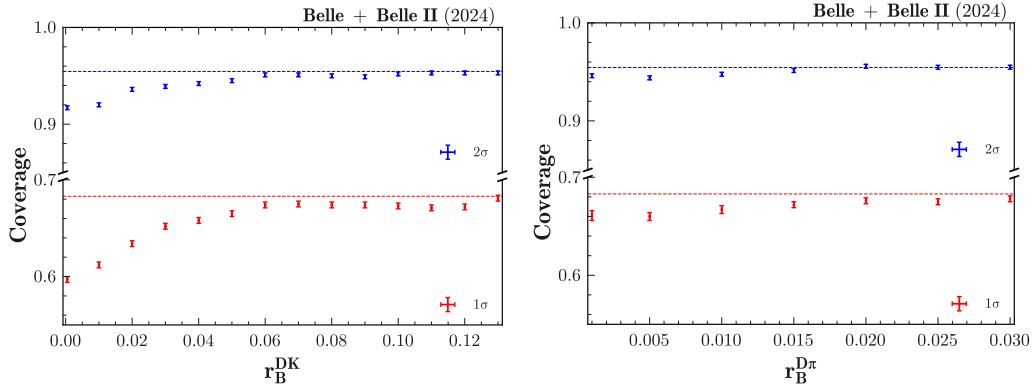


Figure 4. Dependence of the coverage of the ϕ_3 interval on r_B^{DK} (left) and $r_B^{D\pi}$ (right). The dashed horizontal lines show the nominal coverage at 1 (red) and 2σ (blue) for confidence levels of 68.3% and 95.4%, respectively. The y-axis range is split to make the error bars visible.

7 Summary

In summary, we report the value of the CKM angle ϕ_3 by combining existing Belle and Belle II measurements and auxiliary D -decay information from other experiments. This combination includes inputs from a number of $B^+ \rightarrow Dh^+$ and $B^+ \rightarrow D^*K^+$ decay modes. The resulting value for ϕ_3 is $(75.2 \pm 7.6)^\circ$, which is consistent with the world average value within 1.1σ [9]. We obtain higher values of the parameters r_B^{DK} , $r_B^{D\pi}$, and $\delta_B^{D\pi}$ compared to the world average values, with deviations of 1.5σ , 2.2σ , and 4.0σ , respectively. We demonstrate that these differences are likely to be due to our large measured value of $r_B^{D\pi}$. In addition, we achieve a better than anticipated precision on ϕ_3 . This is attributed to the combined effect of a precise $r_D^{K\pi}$ value and larger than expected values of $r_B^{D\pi}$ and $\delta_B^{D\pi}$, which have a significant impact on the ADS ($K^+\pi^-$) final state.

Acknowledgments

This work, based on data collected using the Belle II detector, which was built and commissioned prior to March 2019, and data collected using the Belle detector, which was operated until June 2010, was supported by Higher Education and Science Committee of the Republic of Armenia Grant No. 23LCG-1C011; Australian Research Council and Research Grants No. DP200101792, No. DP210101900, No. DP210102831, No. DE220100462, No. LE210100098, and No. LE230100085; Austrian Federal Ministry of Education, Science and Research, Austrian Science Fund No. P 31361-N36 and No. J4625-N, and Horizon 2020 ERC Starting Grant No. 947006 “InterLeptons”; Natural Sciences and Engineering Research Council of Canada, Compute Canada and CANARIE; National Key R&D Program of China under Contract No. 2022YFA1601903, National Natural Science Foundation of China and Research Grants No. 11575017, No. 11761141009, No. 11705209, No. 11975076, No. 12135005, No. 12150004, No. 12161141008, and No. 12175041, and Shandong Provincial Natural Science Foundation Project ZR2022JQ02; the Czech Science Foundation Grant No. 22-18469S; European Research Council, Seventh Framework PIEF-GA-2013-622527, Horizon 2020 ERC-Advanced Grants No. 267104 and No. 884719, Horizon 2020 ERC-Consolidator Grant No. 819127, Horizon 2020 Marie Skłodowska-Curie Grant Agreement No. 700525 “NIOBE” and No. 101026516, and Horizon 2020 Marie Skłodowska-Curie RISE project JENNIFER2 Grant Agreement No. 822070 (European grants); L’Institut National de Physique Nucléaire et de Physique des Particules (IN2P3) du CNRS and L’Agence Nationale de la Recherche (ANR) under grant ANR-21-CE31-0009 (France); BMBF, DFG, HGF, MPG, and AvH Foundation (Germany); Department of Atomic Energy under Project Identification No. RTI 4002, Department of Science and Technology, and UPES SEED funding programs No. UPES/R&D-SEED-INFRA/17052023/01 and No. UPES/R&D-SOE/20062022/06 (India); Israel Science Foundation Grant No. 2476/17, U.S.-Israel Binational Science Foundation Grant No. 2016113, and Israel Ministry of Science Grant No. 3-16543; Istituto Nazionale di Fisica Nucleare and the Research Grants BELLE2; Japan Society for the Promotion of Science, Grant-in-Aid for Scientific Research Grants No. 16H03968, No. 16H03993, No. 16H06492, No. 16K05323, No. 17H01133, No. 17H05405, No. 18K03621, No. 18H03710, No. 18H05226, No. 19H00682, No. 20H05850, No. 20H05858, No. 22H00144, No. 22K14056, No. 22K21347, No. 23H05433, No. 26220706, and No. 26400255, and the Ministry of Education, Culture, Sports, Science, and Technology (MEXT) of Japan; National Research Foundation (NRF) of Korea Grants No. 2016R1-D1A1B02012900, No. 2018R1A2B3003643, No. 2018R1A6A1A06024970, No. 2019R1I1A3A-01058933, No. 2021R1A6A1A03043957, No. 2021R1F1A1060423, No. 2021R1F1A1064008, No. 2022R1A2C1003993, and No. RS-2022-00197659, Radiation Science Research Institute, Foreign Large-Size Research Facility Application Supporting project, the Global Science Experimental Data Hub Center of the Korea Institute of Science and Technology Information and KREONET/GLORIAD; Universiti Malaya RU grant, Akademi Sains Malaysia, and Ministry of Education Malaysia; Frontiers of Science Program Contracts No. FOINS-296, No. CB-221329, No. CB-236394, No. CB-254409, and No. CB-180023, and SEP-CINVESTAV Research Grant No. 237 (Mexico); the Polish Ministry of Sci-

ence and Higher Education and the National Science Center; the Ministry of Science and Higher Education of the Russian Federation and the HSE University Basic Research Program, Moscow; University of Tabuk Research Grants No. S-0256-1438 and No. S-0280-1439 (Saudi Arabia); Slovenian Research Agency and Research Grants No. J1-9124 and No. P1-0135; Ikerbasque, Basque Foundation for Science, the State Agency for Research of the Spanish Ministry of Science and Innovation through Grant No. PID2022-136510NB-C33, Agencia Estatal de Investigacion, Spain Grant No. RYC2020-029875-I and Generalitat Valenciana, Spain Grant No. CIDEGENT/2018/020; the Swiss National Science Foundation; National Science and Technology Council, and Ministry of Education (Taiwan); Thailand Center of Excellence in Physics; TUBITAK ULAKBIM (Turkey); National Research Foundation of Ukraine, Project No. 2020.02/0257, and Ministry of Education and Science of Ukraine; the U.S. National Science Foundation and Research Grants No. PHY-1913789 and No. PHY-2111604, and the U.S. Department of Energy and Research Awards No. DE-AC06-76RLO1830, No. DE-SC0007983, No. DE-SC0009824, No. DE-SC0009973, No. DE-SC0010007, No. DE-SC0010073, No. DE-SC0010118, No. DE-SC0010504, No. DE-SC0011784, No. DE-SC0012704, No. DE-SC0019230, No. DE-SC0021274, No. DE-SC0021616, No. DE-SC0022350, No. DE-SC0023470; and the Vietnam Academy of Science and Technology (VAST) under Grants No. NVCC.05.12/22-23 and No. DL0000.02/24-25.

These acknowledgements are not to be interpreted as an endorsement of any statement made by any of our institutes, funding agencies, governments, or their representatives.

We thank the SuperKEKB team for delivering high-luminosity collisions; the KEK cryogenics group for the efficient operation of the detector solenoid magnet; the KEK Computer Research Center for on-site computing support; the NII for SINET6 network support; and the raw-data centers hosted by BNL, DESY, GridKa, IN2P3, INFN, PNNL/EMSL, and the University of Victoria.

References

- [1] N. Cabibbo, *Unitary Symmetry and Leptonic Decays*, *Phys. Rev. Lett.* **10** (1963) 531.
- [2] M. Kobayashi and T. Maskawa, *CP Violation in the Renormalizable Theory of Weak Interaction*, *Prog. Theor. Phys.* **49** (1973) 652.
- [3] J. Brod and J. Zupan, *The ultimate theoretical error on γ from $B \rightarrow DK$ decays*, *J. High Energy Phys.* **01** (2014) 051.
- [4] M. Blanke and A.J. Buras, *Emerging ΔM_d -anomaly from tree-level determinations of $|V_{cb}|$ and the angle γ* , *Eur. Phys. J. C* **79** (2019) 159.
- [5] PARTICLE DATA GROUP, *Review of Particle Physics*, *Prog. Theor. Exp. Phys.* **2022** (2022) 083C01.
- [6] LHCb COLLABORATION, *Simultaneous determination of the CKM angle γ and parameters related to mixing and CP violation in the charm sector*, *LHCb-CONF-2024-004* (2024) .
- [7] CKMFITTER GROUP, *Recent CKMfitter updates on global fits of the CKM matrix*, *PoS CKM2021* (2023) 074.
- [8] UTFIT COLLABORATION, *New UFit Analysis of the Unitarity Triangle in the Cabibbo-Kobayashi-Maskawa scheme*, *Rend. Lincei Sci. Fis. Nat.* **34** (2023) 37.
- [9] HEAVY FLAVOR AVERAGING GROUP, *Averages of b-hadron, c-hadron, and τ -lepton properties as of 2021*, *Phys. Rev. D* **107** (2023) 052008.
- [10] G.J. Feldman and R.D. Cousins, *Unified approach to the classical statistical analysis of small signals*, *Phys. Rev. D* **57** (1998) 3873.
- [11] M. Gronau and D. London, *How to determine all the angles of the unitarity triangle from $B_d^0 \rightarrow DK_s$ and $B_s^0 \rightarrow D\phi$* , *Phys. Lett. B* **253** (1991) 483.
- [12] BELLE COLLABORATION, *Study of $B^\pm \rightarrow D_{CP\pm} K^\pm$ and $D_{CP\pm}^* K^\pm$ decays*, *Phys. Rev. D* **73** (2006) 051106.
- [13] D. Atwood, I. Dunietz and A. Soni, *Enhanced CP Violation with $B \rightarrow KD^0(\bar{D}^0)$ Modes and Extraction of the Cabibbo-Kobayashi-Maskawa Angle γ* , *Phys. Rev. Lett.* **78** (1997) 3257.
- [14] D. Atwood, I. Dunietz and A. Soni, *Improved methods for observing CP violation in $B^\pm \rightarrow K^\pm D$ and measuring the CKM phase γ* , *Phys. Rev. D* **63** (2001) 036005.
- [15] BELLE COLLABORATION, *Evidence for the suppressed decay $B^- \rightarrow DK^-$, $D \rightarrow K^+ \pi^- \pi^0$* , *Phys. Rev. D* **88** (2013) 091104.
- [16] BABAR COLLABORATION, *Measurement of CP observables in $B^\pm \rightarrow D_{CP} K^\pm$ decays and constraints on the CKM angle γ* , *Phys. Rev. D* **82** (2010) 072004.
- [17] Y. Grossman, Z. Ligeti and A. Soffer, *Measuring γ in $B^\pm \rightarrow K^\pm(KK^*)_D$ decays*, *Phys. Rev. D* **67** (2003) 071301.
- [18] A. Giri, Y. Grossman, A. Soffer and J. Zupan, *Determining γ using $B^\pm \rightarrow DK^\pm$ with multibody D decays*, *Phys. Rev. D* **68** (2003) 054018.
- [19] A. Bondar and A. Poluektov, *The use of quantum-correlated D^0 decays for ϕ_3 measurement*, *Eur. Phys. J. C* **55** (2008) 51.
- [20] A. Bondar and A. Poluektov, *Feasibility study of model-independent approach to ϕ_3 measurement using Dalitz plot analysis*, *Eur. Phys. J. C* **47** (2006) 347.

- [21] M. Rama, *Effect of $D - \bar{D}$ mixing in the extraction of γ with $B^- \rightarrow D^0 K^-$ and $B^- \rightarrow D^0 \pi^-$ decays*, *Phys. Rev. D* **89** (2014) 014021.
- [22] LHCb COLLABORATION, *Measurement of the Time-Integrated CP Asymmetry in $D^0 \rightarrow K^- K^+$ Decays*, *Phys. Rev. Lett.* **131** (2023) 091802.
- [23] BELLE AND BELLE II COLLABORATIONS, *Measurement of branching-fraction ratios and CP asymmetries in $B^\pm \rightarrow D_{CP^\pm} K^\pm$ decays at Belle and Belle II*, to appear in J. High Energy Phys., *J. High Energy Phys.* **05** (2024) 212.
- [24] BELLE COLLABORATION, *Evidence for the Suppressed Decay $B^- \rightarrow DK^-$, $D \rightarrow K^+ \pi^-$* , *Phys. Rev. Lett.* **106** (2011) 231803.
- [25] BELLE AND BELLE II COLLABORATIONS, *Measurement of CP asymmetries and branching-fraction ratios for $B^\pm \rightarrow DK^\pm$ and $D\pi^\mp$ with $D \rightarrow K_S^0 K^\pm \pi^\mp$ using Belle and Belle II data*, *J. High Energy Phys.* **09** (2023) 146.
- [26] BELLE AND BELLE II COLLABORATIONS, *Combined analysis of Belle and Belle II data to determine the CKM angle using $B^+ \rightarrow D(\rightarrow K_S^0 h^+ h^-)h^+$ decays*, *J. High Energy Phys.* **02** (2022) 063.
- [27] BELLE COLLABORATION, *First measurement of the CKM angle ϕ_3 with $B^\pm \rightarrow D(K_S^0 \pi^+ \pi^- \pi^0)K^\pm$ decays*, *J. High Energy Phys.* **10** (2019) 178.
- [28] BELLE COLLABORATION, *Evidence for direct CP violation in the decay $B^\pm \rightarrow D^{(*)}K^\pm$, $D^0 \rightarrow K_S^0 \pi^+ \pi^-$ and measurement of the CKM phase ϕ_3* , *Phys. Rev. D* **81** (2010) 112002.
- [29] J. Garra Ticó, *A strategy for a simultaneous measurement of CP violation parameters related to the CKM angle γ in multiple B meson decay channels*, [1804.05597](#).
- [30] J. Garra Ticó, V. Gibson, S.C. Haines, C.R. Jones, M. Kenzie and G. Lovell, *Study of the sensitivity to CKM angle γ under simultaneous determination from multiple B meson decay modes*, *Phys. Rev. D* **102** (2020) 053003.
- [31] BELLE COLLABORATION, *Search for the decay $B^0 \rightarrow DK^{*0}$ followed by $D \rightarrow K^- \pi^+$* , *Phys. Rev. D* **86** (2012) 011101.
- [32] BELLE COLLABORATION, *Measurements of time-dependent CP asymmetries in $B \rightarrow D^{*\mp} \pi^\pm$ decays using a partial reconstruction technique*, *Phys. Rev. D* **84** (2011) 021101.
- [33] BELLE COLLABORATION, *First model-independent Dalitz analysis of $B^0 \rightarrow DK^{*0}$, $D \rightarrow K_S^0 \pi^+ \pi^-$ decay*, *Prog. Theor. Exp. Phys.* **2016** (2016) 043C01.
- [34] BESIII COLLABORATION, *Improved measurement of the strong-phase difference $\delta_D^{K\pi}$ in quantum-correlated $D\bar{D}$ decays*, *Eur. Phys. J. C* **82** (2022) 1009.
- [35] BESIII COLLABORATION, *Measurement of the $D \rightarrow K^- \pi^+ \pi^+ \pi^-$ and $D \rightarrow K^- \pi^+ \pi^0$ coherence factors and average strong-phase differences in quantum-correlated $D\bar{D}$ decays*, *J. High Energy Phys.* **05** (2021) 164.
- [36] CLEO COLLABORATION, *Studies of the decays $D^0 \rightarrow K_S^0 K^- \pi^+$ and $D^0 \rightarrow K_S^0 K^+ \pi^-$* , *Phys. Rev. D* **85** (2012) 092016.
- [37] LHCb COLLABORATION, *Studies of the resonance structure in $D^0 \rightarrow K_S^0 K^\pm \pi^\mp$ decays*, *Phys. Rev. D* **93** (2016) 052018.
- [38] LHCb COLLABORATION, *Observation of the Mass Difference Between Neutral Charm-Meson Eigenstates*, *Phys. Rev. Lett.* **127** (2021) 111801.

- [39] BELLE II COLLABORATION, *Snowmass White Paper: Belle II physics reach and plans for the next decade and beyond*, [2207.06307](#).
- [40] LHCb COLLABORATION, *Measurement of the CKM angle γ in $B^\pm \rightarrow DK^\pm$ and $B^\pm \rightarrow D\pi^\pm$ decays with $D \rightarrow K_S^0 h^+ h^-$* , *J. High Energy Phys.* **02** (2021) 169.
- [41] M. Kenzie, M. Martinelli and N. Tuning, *Estimating $r_B^{D\pi}$ as an input to the determination of the CKM angle γ* , *Phys. Rev. D* **94** (2016) 054021.
- [42] LHCb COLLABORATION, *Measurement of the ckm angle γ from a combination of lcb results*, *J. High Energy Phys.* **12** (2016) 087.

A χ^2 of each input measurement

We show the χ^2 value for each input measurement in Table. 7.

Table 7. Auxiliary input observables and their values used in the ϕ_3 combination.

	Measurement	χ^2	No. of obs.
Belle and Belle II	$B^+ \rightarrow Dh^+, D \rightarrow K_S^0 \pi^0, K^- K^+$	7.50	4
	$B^+ \rightarrow Dh^+, D \rightarrow K^+ \pi^-$	1.33	4
	$B^+ \rightarrow Dh^+, D \rightarrow K^+ \pi^- \pi^0$	5.81	4
	$B^+ \rightarrow Dh^+, D \rightarrow K_S^0 K^- \pi^+$	7.52	7
	$B^+ \rightarrow Dh^+ D \rightarrow K_S^0 h^- h^+$	2.07	6
	$B^+ \rightarrow Dh^+, D \rightarrow K_S^0 \pi^- \pi^+ \pi^0$	9.53	8
	$B^+ \rightarrow D^* K^+, D^* \rightarrow D \pi^0, D \rightarrow K_S^0 \pi^0, K_S^0 \phi, K_S^0 \omega, K^- K^+, \pi^- \pi^+$	1.45	4
	$B^+ \rightarrow D^* K^+, D^* \rightarrow D \pi^0, D \gamma, D \rightarrow K_S^0 \pi^- \pi^+$	1.42	8
External	$D \rightarrow K^+ \pi^-$	0.03	2
	$D \rightarrow K^+ \pi^- \pi^0$	0.14	3
	$D - \bar{D}$ mixing	0.02	4
	$D \rightarrow K_S^0 K^- \pi^+$	1.17	4
	R_{GLS}	0.12	1
	Total	38.1	59

B Pull distribution of each input observable

We show the pull of each input observable with respect to the global best-fit point in Figure 5.

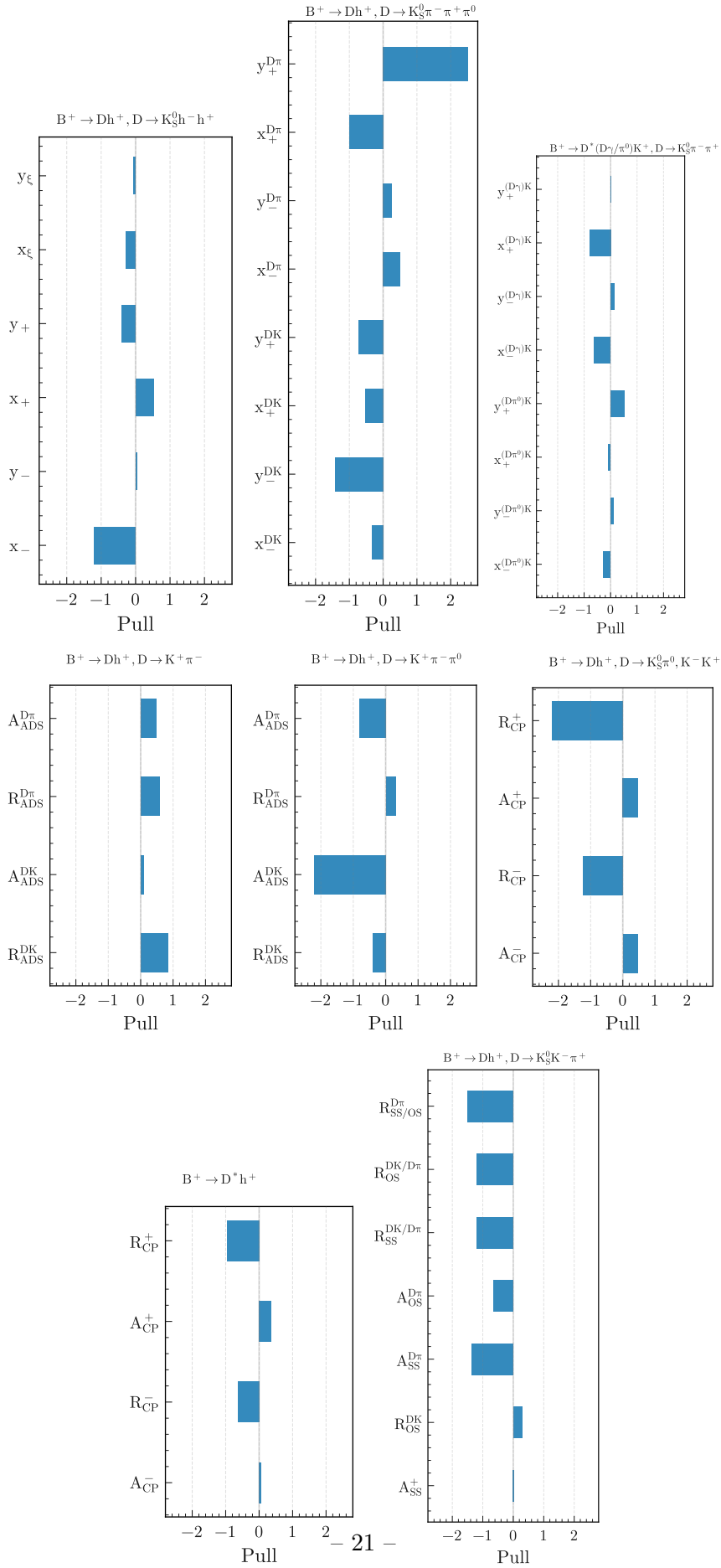


Figure 5. Pulls of the input observables from Belle and Belle II.

C Relationships among parameters and observables

We list the equations that give the relationships among the parameters of interest and observables in the B decay channels. For simplicity, the equations are given in the absence of $D^0 - \bar{D}^0$ mixing. In order to include the small effects from $D^0 - \bar{D}^0$ mixing, the equations should be modified following the recommendation in Ref. [21].

- $B^+ \rightarrow Dh^+, D \rightarrow K_S^0 h^- h^+$ observables

$$\begin{aligned}
x_{\pm}^{DK} &= r_B^{DK} \cos(\delta_B^{DK} \pm \phi_3), \\
y_{\pm}^{DK} &= r_B^{DK} \sin(\delta_B^{DK} \pm \phi_3), \\
x_{\xi}^{D\pi} &= (r_B^{D\pi}/r_B^{DK}) \cos(\delta_B^{D\pi} - \delta_B^{DK}), \\
y_{\xi}^{D\pi} &= (r_B^{D\pi}/r_B^{DK}) \sin(\delta_B^{D\pi} - \delta_B^{DK}).
\end{aligned} \tag{C.1}$$

- $B^+ \rightarrow Dh^+, D \rightarrow K_S^0 \pi^- \pi^+ \pi^0$ observables

$$\begin{aligned}
x_{\pm}^{DK} &= r_B^{DK} \cos(\delta_B^{DK} \pm \phi_3), \\
y_{\pm}^{DK} &= r_B^{DK} \sin(\delta_B^{DK} \pm \phi_3), \\
x_{\pm}^{D\pi} &= r_B^{D\pi} \cos(\delta_B^{D\pi} \pm \phi_3), \\
y_{\pm}^{D\pi} &= r_B^{D\pi} \sin(\delta_B^{D\pi} \pm \phi_3).
\end{aligned} \tag{C.2}$$

- $B^+ \rightarrow D^* K^+, D \rightarrow K_S^0 \pi^- \pi^+$ observables

$$\begin{aligned}
x_{\pm}^{(D\pi^0)K} &= r_B^{D^*K} \cos(\delta_B^{D^*K} \pm \phi_3), \\
y_{\pm}^{(D\pi^0)K} &= r_B^{D^*K} \sin(\delta_B^{D^*K} \pm \phi_3), \\
x_{\pm}^{(D\gamma)K} &= -r_B^{D^*K} \cos(\delta_B^{D^*K} \pm \phi_3), \\
y_{\pm}^{(D\gamma)K} &= -r_B^{D^*K} \sin(\delta_B^{D^*K} \pm \phi_3),
\end{aligned} \tag{C.3}$$

- $B^+ \rightarrow Dh^+, D \rightarrow K^+ \pi^-$ observables

$$\begin{aligned}
R_{\text{ADS}}^{DK, K\pi} &= (r_B^{DK})^2 + (r_D^{K\pi})^2 + 2r_B^{DK} r_D^{K\pi} \cos(\delta_B^{DK} + \delta_D^{K\pi}) \cos \phi_3, \\
A_{\text{ADS}}^{DK, K\pi} &= 2r_B^{DK} r_D^{K\pi} \sin(\delta_B^{DK} + \delta_D^{K\pi}) \sin \phi_3 / R_{\text{ADS}}^{DK, K\pi}, \\
R_{\text{ADS}}^{D\pi, K\pi} &= (r_B^{D\pi})^2 + (r_D^{K\pi})^2 + 2r_B^{D\pi} r_D^{K\pi} \cos(\delta_B^{D\pi} + \delta_D^{K\pi}) \cos \phi_3, \\
A_{\text{ADS}}^{D\pi, K\pi} &= 2r_B^{D\pi} r_D^{K\pi} \sin(\delta_B^{D\pi} + \delta_D^{K\pi}) \sin \phi_3 / R_{\text{ADS}}^{D\pi, K\pi}.
\end{aligned} \tag{C.4}$$

- $B^+ \rightarrow Dh^+, D \rightarrow K^+ \pi^- \pi^0$ observables

$$\begin{aligned}
R_{\text{ADS}}^{DK, K\pi\pi^0} &= (r_B^{DK})^2 + (r_D^{K\pi\pi^0})^2 + 2r_B^{DK} r_D^{K\pi\pi^0} \kappa_D^{K\pi\pi^0} \cos(\delta_B^{DK} + \delta_D^{K\pi\pi^0}) \cos \phi_3, \\
A_{\text{ADS}}^{DK, K\pi\pi^0} &= 2r_B^{DK} r_D^{K\pi\pi^0} \kappa_D^{K\pi\pi^0} \sin(\delta_B^{DK} + \delta_D^{K\pi\pi^0}) \sin \phi_3 / R_{\text{ADS}}^{DK, K\pi\pi^0}, \\
R_{\text{ADS}}^{D\pi, K\pi\pi^0} &= (r_B^{D\pi})^2 + (r_D^{K\pi\pi^0})^2 + 2r_B^{D\pi} r_D^{K\pi\pi^0} \kappa_D^{K\pi\pi^0} \cos(\delta_B^{D\pi\pi^0} + \delta_D^{K\pi\pi^0}) \cos \phi_3, \\
A_{\text{ADS}}^{D\pi, K\pi\pi^0} &= 2r_B^{D\pi} r_D^{K\pi\pi^0} \kappa_D^{K\pi\pi^0} \sin(\delta_B^{D\pi\pi^0} + \delta_D^{K\pi\pi^0}) \sin \phi_3 / R_{\text{ADS}}^{D\pi, K\pi\pi^0}.
\end{aligned} \tag{C.5}$$

- $B^+ \rightarrow Dh^+, D \rightarrow K_S^0 \pi^0, K^- K^+$ observables

$$\begin{aligned} \mathcal{R}_{CP\pm} &= 1 + (r_B^{DK})^2 + 2\eta_{CP} r_B^{DK} \cos(\delta_B^{DK}) \cos \phi_3, \\ A_{CP\pm} &= 2\eta_{CP} r_B^{DK} \sin(\delta_B^{DK}) \sin \phi_3 / \mathcal{R}_{CP\pm}, \end{aligned} \quad (\text{C.6})$$

where η_{CP} denotes the CP eigenvalue of the D decay.

- $B^+ \rightarrow D^* h^+, D \rightarrow K_S^0 \pi^0, K^- K^+, K_S^0 \phi, K_S^0 \omega, \pi^- \pi^+$ observables

$$\begin{aligned} \mathcal{R}_{CP\pm} &= 1 + (r_B^{D^*K})^2 + 2\eta_{CP} r_B^{D^*K} \cos(\delta_B^{D^*K}) \cos \phi_3, \\ A_{CP\pm} &= 2\eta_{CP} r_B^{D^*K} \sin(\delta_B^{D^*K}) \sin \phi_3 / \mathcal{R}_{CP\pm}. \end{aligned} \quad (\text{C.7})$$

- $B^+ \rightarrow Dh^+, D \rightarrow K_S^0 K^- \pi^+$ observables

$$\begin{aligned} A_{SS}^{DK} &= \frac{2r_B^{DK} r_D^{K_S^0 K \pi} \kappa_D^{K_S^0 K \pi} \sin(\delta_B^{DK} - \delta_D^{K_S^0 K \pi}) \sin \phi_3}{1 + (r_B^{DK})^2 (r_D^{K_S^0 K \pi})^2 + 2r_B^{DK} r_D^{K_S^0 K \pi} \kappa_D^{K_S^0 K \pi} \cos(\delta_B^{DK} - \delta_D^{K_S^0 K \pi}) \cos \phi_3}, \\ A_{OS}^{DK} &= \frac{2r_B^{DK} r_D^{K_S^0 K \pi} \kappa_D^{K_S^0 K \pi} \sin(\delta_B^{DK} + \delta_D^{K_S^0 K \pi}) \sin \phi_3}{(r_B^{DK})^2 + (r_D^{K_S^0 K \pi})^2 + 2r_B^{DK} r_D^{K_S^0 K \pi} \kappa_D^{K_S^0 K \pi} \cos(\delta_B^{DK} + \delta_D^{K_S^0 K \pi}) \cos \phi_3}, \\ A_{SS}^{D\pi} &= \frac{2r_B^{D\pi} r_D^{K_S^0 K \pi} \kappa_D^{K_S^0 K \pi} \sin(\delta_B^{D\pi} - \delta_D^{K_S^0 K \pi}) \sin \phi_3}{1 + (r_B^{D\pi})^2 (r_D^{K_S^0 K \pi})^2 + 2r_B^{D\pi} r_D^{K_S^0 K \pi} \kappa_D^{K_S^0 K \pi} \cos(\delta_B^{D\pi} - \delta_D^{K_S^0 K \pi}) \cos \phi_3}, \\ A_{OS}^{D\pi} &= \frac{2r_B^{D\pi} r_D^{K_S^0 K \pi} \kappa_D^{K_S^0 K \pi} \sin(\delta_B^{D\pi} + \delta_D^{K_S^0 K \pi}) \sin \phi_3}{(r_B^{D\pi})^2 + (r_D^{K_S^0 K \pi})^2 + 2r_B^{D\pi} r_D^{K_S^0 K \pi} \kappa_D^{K_S^0 K \pi} \cos(\delta_B^{D\pi} + \delta_D^{K_S^0 K \pi}) \cos \phi_3}, \\ R_{SS}^{DK/D\pi} &= R_{\text{GLS}} \frac{1 + (r_B^{DK})^2 (r_D^{K_S^0 K \pi})^2 + 2r_B^{DK} r_D^{K_S^0 K \pi} \kappa_D^{K_S^0 K \pi} \cos(\delta_B^{DK} - \delta_D^{K_S^0 K \pi}) \cos \phi_3}{1 + (r_B^{D\pi})^2 (r_D^{K_S^0 K \pi})^2 + 2r_B^{D\pi} r_D^{K_S^0 K \pi} \kappa_D^{K_S^0 K \pi} \cos(\delta_B^{D\pi} - \delta_D^{K_S^0 K \pi}) \cos \phi_3}, \\ R_{OS}^{DK/D\pi} &= R_{\text{GLS}} \frac{(r_B^{DK})^2 + (r_D^{K_S^0 K \pi})^2 + 2r_B^{DK} r_D^{K_S^0 K \pi} \kappa_D^{K_S^0 K \pi} \cos(\delta_B^{DK} + \delta_D^{K_S^0 K \pi}) \cos \phi_3}{(r_B^{D\pi})^2 + (r_D^{K_S^0 K \pi})^2 + 2r_B^{D\pi} r_D^{K_S^0 K \pi} \kappa_D^{K_S^0 K \pi} \cos(\delta_B^{D\pi} + \delta_D^{K_S^0 K \pi}) \cos \phi_3}, \\ R_{SS/OS}^{D\pi} &= \frac{1 + (r_B^{D\pi})^2 (r_D^{K_S^0 K \pi})^2 + 2r_B^{D\pi} r_D^{K_S^0 K \pi} \kappa_D^{K_S^0 K \pi} \cos(\delta_B^{D\pi} - \delta_D^{K_S^0 K \pi}) \cos \phi_3}{(r_B^{D\pi})^2 + (r_D^{K_S^0 K \pi})^2 + 2r_B^{D\pi} r_D^{K_S^0 K \pi} \kappa_D^{K_S^0 K \pi} \cos(\delta_B^{D\pi} + \delta_D^{K_S^0 K \pi}) \cos \phi_3}. \end{aligned} \quad (\text{C.8})$$

D Input observable values, uncertainties, and uncertainties correlations

We list the input observables' values, uncertainties, as well as correlations between uncertainties.

D.1 $B^+ \rightarrow Dh^+, D \rightarrow K_S^0 h^- h^+$ analysis

The values and uncertainties are taken from Ref. [26]. These are

$$\begin{aligned}
x_-^{DK} &= 0.0924 \pm 0.0327 \pm 0.0029, \\
y_-^{DK} &= 0.1000 \pm 0.0420 \pm 0.0074, \\
x_+^{DK} &= -0.1128 \pm 0.0315 \pm 0.0029, \\
y_+^{DK} &= -0.0455 \pm 0.0420 \pm 0.0055, \\
x_\xi^{D\pi} &= -0.1109 \pm 0.0475 \pm 0.0085, \\
y_\xi^{D\pi} &= -0.0790 \pm 0.0544 \pm 0.0083,
\end{aligned} \tag{D.1}$$

where the first uncertainty is statistical and the second one includes systematic uncertainty and the additional uncertainty from the strong-interaction phase difference in $D \rightarrow K_s^0 \pi^+ \pi^-$ decays. The statistical and systematic correlation matrices are given in Tables 8 and 9.

Table 8. Correlation matrix of the statistical uncertainties for the $B^+ \rightarrow Dh^+, D \rightarrow K_s^0 h^- h^+$ observables.

	x_-^{DK}	y_-^{DK}	x_+^{DK}	y_+^{DK}	$x_\xi^{D\pi}$	$y_\xi^{D\pi}$
x_-^{DK}	1.000	-0.204	-0.051	0.063	0.365	-0.151
y_-^{DK}		1.000	0.014	-0.051	-0.090	0.404
x_+^{DK}			1.000	0.152	-0.330	-0.057
y_+^{DK}				1.000	0.026	-0.391
$x_\xi^{D\pi}$					1.000	0.080
$y_\xi^{D\pi}$						1.000

Table 9. Correlation matrix of the systematic uncertainties for the $B^+ \rightarrow Dh^+, D \rightarrow K_s^0 h^- h^+$ observables.

	x_-^{DK}	y_-^{DK}	x_+^{DK}	y_+^{DK}	$x_\xi^{D\pi}$	$y_\xi^{D\pi}$
x_-^{DK}	1.000	0.104	0.228	0.335	0.248	0.145
y_-^{DK}		1.000	0.199	-0.119	-0.410	-0.103
x_+^{DK}			1.000	0.423	0.063	-0.375
y_+^{DK}				1.000	0.173	-0.089
$x_\xi^{D\pi}$					1.000	0.566
$y_\xi^{D\pi}$						1.000

D.2 $B^+ \rightarrow Dh^+, D \rightarrow K_s^0 \pi^- \pi^+ \pi^0$ analysis

The values and uncertainties are taken from Ref. [27]. Those are

$$\begin{aligned}
x_-^{DK} &= 0.095 \pm 0.121 \pm 0.029, \\
y_-^{DK} &= 0.354 \pm 0.170 \pm 0.045, \\
x_+^{DK} &= -0.030 \pm 0.121 \pm 0.026, \\
y_+^{DK} &= 0.220 \pm 0.376 \pm 0.079, \\
x_-^{D\pi} &= -0.014 \pm 0.021 \pm 0.021, \\
y_-^{D\pi} &= -0.033 \pm 0.059 \pm 0.023, \\
x_+^{D\pi} &= 0.039 \pm 0.024 \pm 0.020, \\
y_+^{D\pi} &= -0.196 \pm 0.069 \pm 0.048,
\end{aligned} \tag{D.2}$$

where the first uncertainty is statistical and the second one includes systematic uncertainty and the additional uncertainty from the strong-interaction phase difference in $D \rightarrow K_s^0 \pi^+ \pi^- \pi^0$ decays. The statistical correlation matrix is given in Table 10. The systematic correlation matrix was not reported for this measurement.

Table 10. Correlation matrix of the statistical uncertainties for the $B^+ \rightarrow Dh^+$, $D \rightarrow K_s^0 \pi^- \pi^+ \pi^0$ observables.

	x_-^{DK}	y_-^{DK}	x_+^{DK}	y_+^{DK}	$x_-^{D\pi}$	$y_-^{D\pi}$	$x_+^{D\pi}$	$y_+^{D\pi}$
x_-^{DK}	1.000	0.486	0.172	-0.231	0.000	0.000	0.000	0.000
y_-^{DK}		1.000	-0.127	0.179	0.000	0.000	0.000	0.000
x_+^{DK}			1.000	0.365	0.000	0.000	0.000	0.000
y_+^{DK}				1.000	0.000	0.000	0.000	0.000
$x_-^{D\pi}$					1.000	-0.364	0.314	0.050
$y_-^{D\pi}$						1.000	0.347	0.055
$x_+^{D\pi}$							1.000	-0.032
$y_+^{D\pi}$								1.000

D.3 $B^+ \rightarrow D^* K^+$, $D \rightarrow K_s^0 \pi^- \pi^+$ analysis

The values and uncertainties are taken from Ref. [28]. Those are

$$\begin{aligned}
x_-^{(D\pi^0)K} &= 0.024 \pm 0.140 \pm 0.018, \\
y_-^{(D\pi^0)K} &= -0.243 \pm 0.137 \pm 0.022, \\
x_+^{(D\pi^0)K} &= 0.133 \pm 0.083 \pm 0.018, \\
y_+^{(D\pi^0)K} &= 0.130 \pm 0.120 \pm 0.022, \\
x_-^{(D\gamma)K} &= 0.144 \pm 0.208 \pm 0.025, \\
y_-^{(D\gamma)K} &= 0.196 \pm 0.215 \pm 0.037, \\
x_+^{(D\gamma)K} &= -0.006 \pm 0.147 \pm 0.025, \\
y_+^{(D\gamma)K} &= -0.190 \pm 0.177 \pm 0.037,
\end{aligned} \tag{D.3}$$

where the first uncertainty is statistical and the second one systematic. The uncertainty from the $D \rightarrow K_S^0 \pi^+ \pi^-$ decay model is unknown. The statistical correlation matrix is given in Table 11. The systematic correlation matrix was not reported for this measurement.

Table 11. Correlation matrix of the statistical uncertainties for the $B^+ \rightarrow D^* K^+, D^* \rightarrow D\pi^0/\gamma, D \rightarrow K_S^0 \pi^- \pi^+$ observables.

	$x_-^{(D\pi^0)K}$	$y_-^{(D\pi^0)K}$	$x_+^{(D\pi^0)K}$	$y_+^{(D\pi^0)K}$	$x_-^{(D\gamma)K}$	$y_-^{(D\gamma)K}$	$x_+^{(D\gamma)K}$	$y_+^{(D\gamma)K}$
$x_-^{(D\pi^0)K}$	1.000	0.440	0.000	0.000	0.000	0.000	0.000	0.000
$y_-^{(D\pi^0)K}$		1.000	0.000	0.000	0.000	0.000	0.000	0.000
$x_+^{(D\pi^0)K}$			1.000	-0.101	0.000	0.000	0.000	0.000
$y_+^{(D\pi^0)K}$				1.000	0.000	0.000	0.000	0.000
$x_-^{(D\gamma)K}$					1.000	-0.207	0.000	0.000
$y_-^{(D\gamma)K}$						1.000	0.000	0.000
$x_+^{(D\gamma)K}$							1.000	0.080
$y_+^{(D\gamma)K}$								1.000

D.4 $B^+ \rightarrow Dh^+, D \rightarrow K^+ \pi^-$ analysis

The values and uncertainties are taken from Ref. [24]. Those are

$$\begin{aligned}
R_{K\pi}^{DK} &= 0.0163 \pm 0.0042 \pm 0.0010, \\
A_{K\pi}^{DK} &= -0.39 \pm 0.27 \pm 0.04, \\
R_{K\pi}^{D\pi} &= 0.00328 \pm 0.00037 \pm 0.00015, \\
A_{K\pi}^{D\pi} &= -0.04 \pm 0.11 \pm 0.02,
\end{aligned}
\tag{D.4}$$

where the first uncertainty is statistical and the second one systematic. The statistical correlation matrix is given in Table 12. The systematic correlation matrix was not reported for this measurement.

Table 12. Correlation matrix of the statistical uncertainties for the $B^+ \rightarrow Dh^+, D \rightarrow K^+ \pi^-$ observables.

	$R_{K\pi}^{DK}$	$A_{K\pi}^{DK}$	$R_{K\pi}^{D\pi}$	$A_{K\pi}^{D\pi}$
$R_{K\pi}^{DK}$	1.000	0.242	0.000	0.000
$A_{K\pi}^{DK}$		1.000	0.000	0.000
$R_{K\pi}^{D\pi}$			1.000	-0.032
$A_{K\pi}^{D\pi}$				1.000

D.5 $B^+ \rightarrow Dh^+, D \rightarrow K^+\pi^-\pi^0$ analysis

The values and uncertainties are taken from Ref. [15]. Those are

$$\begin{aligned}
R_{K\pi\pi^0}^{DK} &= (1.98 \pm 0.62 \pm 0.24) \times 10^{-2}, \\
A_{K\pi\pi^0}^{DK} &= 0.41 \pm 0.307 \pm 0.05, \\
R_{K\pi\pi^0}^{D\pi} &= (0.19 \pm 0.05 \pm 0.02) \times 10^{-2}, \\
A_{K\pi\pi^0}^{D\pi} &= 0.16 \pm 0.27 \pm 0.04,
\end{aligned}
\tag{D.5}$$

where the first uncertainty is statistical and the second one systematic. The statistical and systematic correlation matrices were not reported for this measurement.

D.6 $B^+ \rightarrow Dh^+, D \rightarrow K_s^0\pi^0, K^-K^+$ analysis

The values and uncertainties are taken from Ref. [23]. Those are

$$\begin{aligned}
A_{CP-}^{DK} &= -0.167 \pm 0.057 \pm 0.006, \\
R_{CP-}^{DK} &= 1.151 \pm 0.074 \pm 0.019, \\
A_{CP+}^{DK} &= 0.125 \pm 0.058 \pm 0.014, \\
R_{CP+}^{DK} &= 1.164 \pm 0.081 \pm 0.036,
\end{aligned}
\tag{D.6}$$

where the first uncertainty is statistical and the second one systematic. The statistical and systematic correlation matrices are given in Tables 13 and 14.

Table 13. Correlation matrix of the statistical uncertainties for the $B^+ \rightarrow DK^+, D \rightarrow K_s^0\pi^0, K^-K^+$ observables.

	A_{CP-}^{DK}	R_{CP-}^{DK}	A_{CP+}^{DK}	R_{CP+}^{DK}
A_{CP-}^{DK}	1.000	0.056	0.000	0.000
R_{CP-}^{DK}		1.000	0.000	-0.081
A_{CP+}^{DK}			1.000	0.060
R_{CP+}^{DK}				1.000

Table 14. Correlation matrix of the systematic uncertainties for the $B^+ \rightarrow DK^+, D \rightarrow K_s^0\pi^0, K^-K^+$ observables.

	A_{CP-}^{DK}	R_{CP-}^{DK}	A_{CP+}^{DK}	R_{CP+}^{DK}
A_{CP-}^{DK}	1.000	-0.490	0.540	0.005
R_{CP-}^{DK}		1.000	-0.128	-0.063
A_{CP+}^{DK}			1.000	0.342
R_{CP+}^{DK}				1.000

D.7 $B^+ \rightarrow D^*h^+, D \rightarrow K_s^0\pi^0, K^-K^+, K_s^0\phi, K_s^0\omega, \pi^-\pi^+$ analysis

The values and uncertainties are taken from Ref. [12]. Those are

$$\begin{aligned}
A_{CP-}^{DK} &= 0.13 \pm 0.30 \pm 0.08, \\
R_{CP-}^{DK} &= 1.15 \pm 0.31 \pm 0.12, \\
A_{CP+}^{DK} &= -0.20 \pm 0.22 \pm 0.04, \\
R_{CP+}^{DK} &= 1.41 \pm 0.25 \pm 0.06,
\end{aligned} \tag{D.7}$$

where the first uncertainty is statistical and the second one systematic. The statistical and systematic correlation matrices were not reported for this measurement.

D.8 $B^+ \rightarrow Dh^+, D \rightarrow K_s^0K^-\pi^+$ analysis

The values and uncertainties are taken from Ref. [25]. Those are

$$\begin{aligned}
A_{SS}^{DK} &= 0.055 \pm 0.119 \pm 0.020, \\
A_{OS}^{DK} &= 0.231 \pm 0.184 \pm 0.014, \\
A_{SS}^{D\pi} &= 0.046 \pm 0.029 \pm 0.016, \\
A_{OS}^{D\pi} &= 0.009 \pm 0.046 \pm 0.009, \\
R_{SS}^{DK/D\pi} &= 0.093 \pm 0.012 \pm 0.005, \\
R_{OS}^{DK/D\pi} &= 0.103 \pm 0.020 \pm 0.006, \\
R_{SS/OS}^{D\pi} &= 2.412 \pm 0.132 \pm 0.019,
\end{aligned} \tag{D.8}$$

where the first uncertainty is statistical and the second one systematic. The statistical and systematic correlation matrices are given in Tables 15 and 16.

Table 15. Correlation matrix of the statistical uncertainties for the $B^+ \rightarrow Dh^+, D \rightarrow K_s^0K^-\pi^+$ observables.

	A_{SS}^{DK}	A_{OS}^{DK}	$A_{SS}^{D\pi}$	$A_{OS}^{D\pi}$	$R_{SS}^{DK/D\pi}$	$R_{OS}^{DK/D\pi}$	$R_{SS/OS}^{D\pi}$
A_{SS}^{DK}	1.000	0.003	-0.012	0.001	-0.052	-0.013	0.002
A_{OS}^{DK}		1.000	0.001	-0.011	-0.004	-0.034	0.002
$A_{SS}^{D\pi}$			1.000	0.001	0.002	-0.004	-0.011
$A_{OS}^{D\pi}$				1.000	-0.002	-0.002	0.014
$R_{SS}^{DK/D\pi}$					1.000	0.034	-0.133
$R_{OS}^{DK/D\pi}$						1.000	0.208
$R_{SS/OS}^{D\pi}$							1.000

Table 16. Correlation matrix of the statistical uncertainties for the $B^+ \rightarrow Dh^+, D \rightarrow K_s^0 K^- \pi^+$ observables.

	A_{SS}^{DK}	A_{OS}^{DK}	$A_{SS}^{D\pi}$	$A_{OS}^{D\pi}$	$R_{SS}^{DK/D\pi}$	$R_{OS}^{DK/D\pi}$	$R_{SS/OS}^{D\pi}$
A_{SS}^{DK}	1.000	0.195	0.047	0.013	0.120	-0.053	0.192
A_{OS}^{DK}		1.000	0.038	0.004	0.344	0.210	0.007
$A_{SS}^{D\pi}$			1.000	0.024	-0.004	-0.037	0.018
$A_{OS}^{D\pi}$				1.000	-0.017	-0.024	0.006
$R_{SS}^{DK/D\pi}$					1.000	0.915	0.015
$R_{OS}^{DK/D\pi}$						1.000	-0.097
$R_{SS/OS}^{D\pi}$							1.000

E External inputs' values, uncertainties, and uncertainties correlations

E.1 Inputs from global fit to $D^0 - \bar{D}^0$ mixing data

The values and uncertainties are taken from Ref. [9]. Those are

$$\begin{aligned}
 x_D &= (0.407 \pm 0.044)\%, \\
 y_D &= (0.647 \pm 0.024)\%, \\
 \delta_D^{K\pi} &= (191.7 \pm 3.7)^\circ, \\
 (r_D^{K\pi})^2 &= (3.44 \pm 0.02) \times 10^{-3},
 \end{aligned} \tag{E.1}$$

where the uncertainty includes both statistical and systematic uncertainties. The correlation matrix is given in Table 17.

Table 17. Correlation matrix for all uncertainties of the input variables from global fit to $D^0 - \bar{D}^0$ mixing data.

	x_D	y_D	$\delta_D^{K\pi}$	$(r_D^{K\pi})^2$
x_D	1.000	-0.030	-0.049	0.023
y_D		1.000	0.867	0.145
$\delta_D^{K\pi}$			1.000	0.534
$(r_D^{K\pi})^2$				1.000

E.2 Input for $D \rightarrow K^+ \pi^-$

The values and uncertainties are taken from Ref. [34]. Those are

$$\begin{aligned}
 r_D^{K\pi} \cos(\delta_D^{K\pi}) &= -0.0562 \pm 0.0081 \pm 0.0051, \\
 r_D^{K\pi} \sin(\delta_D^{K\pi}) &= -0.011 \pm 0.012 \pm 0.0076,
 \end{aligned} \tag{E.2}$$

where the first uncertainty is statistical and the second one systematic. The correlation between these two quantities is 0.02.

E.3 Input for $D \rightarrow K^+ \pi^- \pi^0$

The values and uncertainties are taken from [35]. The values used are

$$\begin{aligned} r_D^{K\pi\pi^0} &= 0.0441 \pm 0.0011 \\ \kappa_D^{K\pi\pi^0} &= 0.79 \pm 0.04, \\ \delta_D^{K\pi\pi^0} &= (196 \pm 11)^\circ, \end{aligned} \tag{E.3}$$

where the uncertainty includes both statistical and systematic uncertainties. The correlation matrix is given in Table 18.

Table 18. Correlation matrix for all uncertainties of the $D \rightarrow K^+ \pi^- \pi^0$ channel parameters.

	$R_D^{K\pi\pi^0}$	$\delta_D^{K\pi\pi^0}$	$r_D^{K\pi\pi^0}$
$R_D^{K\pi\pi^0}$	1.00	0.19	-0.01
$\delta_D^{K\pi\pi^0}$		1.00	0.25
$r_D^{K\pi\pi^0}$			1.00

E.4 Input for $D \rightarrow K_S^0 K^- \pi^+$

The values and uncertainties are taken from Ref. [36]. Those are

$$\begin{aligned} (r_D^{K_S^0 K\pi})^2 &= 0.356 \pm 0.034 \pm 0.007, \\ \kappa_D^{K_S^0 K\pi} &= 0.94 \pm 0.12, \\ \delta_D^{K_S^0 K\pi} &= (-16.6 \pm 18.4)^\circ. \end{aligned} \tag{E.4}$$

For $(r_D^{K_S^0 K\pi})^2$, the first uncertainty is statistical, and the second one is systematic. For $\kappa_D^{K_S^0 K\pi}$ and $\delta_D^{K_S^0 K\pi}$, the uncertainty includes both statistical and systematic uncertainties. The correlation matrix is given in Table 19.

Table 19. Correlation matrix for all uncertainties of the $D \rightarrow K_S^0 K^- \pi^+$ channel parameters from CLEO.

	$(r_D^{K_S^0 K\pi})^2$	$\delta_D^{K_S^0 K\pi}$	$\kappa_D^{K_S^0 K\pi}$
$(r_D^{K_S^0 K\pi})^2$	1.0	0.0	0.0
$\delta_D^{K_S^0 K\pi}$		1.0	-0.6
$\kappa_D^{K_S^0 K\pi}$			1.0

In addition, the following input from Ref. [37] is used,

$$(r_D^{K_S^0 K\pi})^2 = 0.370 \pm 0.003 \pm 0.012, \tag{E.5}$$

where the first uncertainty is statistical and the second one systematic. The value

$$R(\mathcal{B}(B^- \rightarrow D^0 K^-)/\mathcal{B}(B^- \rightarrow D^0 \pi^-)) = 0.0789 \pm 0.0027 \quad (\text{E.6})$$

from the PDG [5] is also used, where the uncertainty includes both statistical and systematic uncertainties.